Hindawi
Mathematical Problems in Engineering
Volume 2020, Article ID 6753949, 23 pages
https://doi.org/10.1155/2020/6753949

Research Article

Research on Fault Feature Extraction Method Based on FDM-RobustICA and MOMEDA

Jingzong Yang,[1] **Xuefeng Li**,[2] **and Limei Wu**[1]

[1]*School of Information, Baoshan University, Baoshan 678000, China*
[2]*School of Transportation, Southeast University, Nanjing 211189, China*

Correspondence should be addressed to Jingzong Yang; yjingzong@foxmail.com

Received 13 April 2020; Revised 22 May 2020; Accepted 28 May 2020; Published 22 June 2020

Academic Editor: Stylianos Georgantzinos

Aiming at the difficulty of extracting rolling bearing fault features under strong background noise conditions, a method based on the Fourier decomposition method (FDM), robust independent component analysis (RobustICA), and multipoint optimal minimum entropy deconvolution adjusted (MOMEDA) is proposed. Firstly, the FDM method is introduced to decompose the single-channel bearing fault signal into several Fourier intrinsic band functions (FIBF). Secondly, by setting the cross-correlation coefficient and kurtosis as a new selection criterion, it can effectively construct the virtual noise channel and the observation signal channel, which makes RobustICA complete the separation of the useful signal and noise well. Finally, MOMEDA is introduced to enhance the periodic impact components in the denoised signal, and then the filtered signal is analyzed by the Hilbert envelope spectrum to extract the fault characteristic frequency. Through the experimental analysis of the simulated signals and the actual bearing fault signals, the results show that the proposed method not only has the ability to suppress noise and accurately extract fault feature information but also has better performance than the traditional method of local mean decomposition (LMD) and intrinsic time-scale decomposition (ITD), highlighting its practicality in the fault diagnosis of rotating machinery.

1. Introduction

Bearing is one of the important parts in the mechanical system, which has been widely used in metallurgy, electric power, aerospace, and other fields of national economy. At the same time, due to the high frequency of use and complex working environment, bearings are also the most prone to failure components. Once it breaks down, it will not only affect the normal operation of the mechanical system but also greatly reduce the production efficiency, even cause the loss of life and property. Therefore, it is very important to extract the fault features of bearings and grasp the operation status of the equipment in time. However, in actual operating conditions, due to the impact of the component's own structure and working environment, the collected signal contains both useful information about bearing failure and useless interference noise. Meanwhile, because the signal passes through many links in the process of transmission, some signals will be attenuated to a certain extent. Affected by the aforementioned adverse factors, the signal-to-noise ratio of the signals collected by the sensor is very low, and the fault characteristics are weak, making it difficult to diagnose the fault. Therefore, how to effectively extract the fault characteristics of bearings is the current research hotspot and difficult point.

At present, most traditional rolling bearing fault feature extraction methods are developed based on time-frequency analysis methods. In the field of fault diagnosis, there are many common methods, such as short-time Fourier transform [1, 2], Wigner–Ville distribution [3], and wavelet transform [4, 5]. Although the above methods have been widely used, they are basically based on the idea of integral analysis. Since the set basis functions are fixed, the signals cannot be decomposed adaptively. This prevents the noise spectrum from being effectively separated during signal processing and may also filter out sudden changes in the signal. To solve the above problem, Huang et al. [6] proposed the empirical mode decomposition (EMD) method, which

can adaptively decompose the signal into several natural modal components, thereby obtaining the complete time-frequency distribution of the signal. It shows some advantages when processing stationary and nonstationary signals, but EMD has problems such as endpoint effects and modal aliasing and lacks strict theoretical proofs [7–9]. In view of the shortcomings of EMD, relevant scholars proposed EEMD, CEEMD, CEEMDAN, and other improved methods, but these methods still have similar problems with EMD [10–12]. Based on the idea of EMD, LMD, ITD, and other signal processing methods have been proposed one after another [13, 14], but these methods cannot fully make up for the shortcomings of EMD. In recent years, Singh et al. [15] proposed a new signal analysis method-Fourier decomposition method (FDM) based on the study of Fourier transform. By using the FDM, any complex signal can be adaptively decomposed into a series of Fourier intrinsic band functions (FIBF). This method changes the defect that the Fourier series expansion method can only handle stationary linear signals and can effectively analyze nonstationary nonlinear signals. Because the FDM is a complete and orthogonal signal processing method with strict theoretical basis, it has been initially applied in fault diagnosis in various fields and has shown great advantages. Dou and Lin [16] demonstrated the adaptive narrowband filtering characteristics of the FDM at low and high frequencies by detecting white Gaussian noise. At the same time, after comparing the effects of different methods on processing gearbox vibration signals, the results show that the FDM can overcome the bottleneck of the EMD in adaptively separating low-frequency signal components and has superior performance. Aiming at the problem that the traditional time-frequency analysis method is difficult to effectively extract the rotor fault characteristics, Liu et al. [17] introduced the FDM to the fault diagnosis of rotor rubbing. Through experimental comparison based on different methods, the results show that the FDM can achieve complete signal decomposition and achieve better fault diagnosis. Fu and Gao [18] proposed a fault diagnosis method for rolling bearings by combining the FDM and singular value difference spectrum. The experimental simulation and actual engineering tests verify the effectiveness of the proposed method.

At the same time, as a blind source separation method, independent component analysis (ICA) provides a new idea for noise reduction of mechanical equipment fault signals. In 1994, Comon explained the concept of independent component analysis (ICA) and pointed out that ICA is an extension of PCA. He proposed the target function of the Kullback–Leibler criterion on the basis of making full use of the high-order statistical characteristics of the signal, which became the mainstream algorithm of blind source separation in the future [19]. After that, the Finnish scholar Hyvarinen and Oja [20] proposed a fast-independent component analysis method based on kurtosis. Then, the algorithm is improved, using more robust negative entropy as a non-Gaussian measurement criterion, and a fast algorithm, FastICA, based on negative entropy maximization is proposed [21]. The algorithm has a very high efficiency, so it has been widely used. However, in 2004, Zarzoso and Comon et al. proposed in [22] that FastICA would fail in the case of weak or high spatial correlation source signals. After that, they put forward the RobustICA [23, 24], and it has developed rapidly in the algorithm of blind source separation. As an algorithm based on kurtosis and optimal step size, this algorithm has excellent antinoise performance. It can separate noise and real signal from the multichannel mixed signal without prior knowledge of the signal source. The algorithm is proved to be not only simple but also better than FastICA. In recent years, it has been successfully applied to the noise source separation in the fields of diesel engine, gasoline engine, and combustion engine [25–29] and has shown high signal separation quality and fast calculation efficiency. However, in the process of using RobustICA, the number of sensors must be greater than or equal to the number of components separated by them [30]. In order to solve the shortcomings of RobustICA, the signal can be decomposed into many components by time-frequency analysis, and more virtual observation channels than the source signal can be generated. In this way, by combining the advantages of the above two methods, noise reduction of the bearing signal can be achieved. However, in the process of use, although the signal-to-noise ratio is improved by suppressing the noise, the useful signal is inevitably suppressed. Especially under the condition of strong noise interference, the impact component of the bearing fault signal after noise reduction is still weak, and even the weak fault may be covered by the strong fault, which brings difficulties for further extraction of fault features.

The essence of fault feature extraction is to extract the periodic shock components in the signal, that is, to process the signal through an optimal filter, thereby highlighting the fault shock components. The minimum entropy deconvolution (MED) was first proposed by Wiggins in 1978 [31]. It uses the maximum kurtosis as the iteration termination condition to solve the filter, which can play a role in highlighting the impact characteristics in the signal [32, 33]. Sawalhi et al. first used MED for fault detection of rotating machinery [34]. However, this iterative method is not only complex but also not necessarily the global optimal filter. Secondly, the method is only suitable for the single pulse impulse signal. The fault characteristics of rotating machinery are mostly periodic pulses. In order to overcome the shortcomings of MED, McDonald et al. proposed the maximum correlated kurtosis deconvolution (MCKD) [35] in 2012 based on the correlation kurtosis. To some extent, this method can satisfy the need of deconvolution with periodic pulse, but it is still an iterative process with the maximum correlation kurtosis as the criterion. The result is not the optimal solution, and it needs the prior knowledge of the fault cycle. In view of the limitations of the above two methods, McDonald and Zhao [36] proposed the multipoint optimal minimum entropy deconvolution adjusted (MOMEDA), which has been successfully applied to the fault diagnosis of the gearbox. This method uses a time target vector to define the pulse position obtained by solving the deconvolution. During the execution of the algorithm, the optimal filter can be obtained without iteration [37], and the period of the failure does not need to be determined in

advance. By using this method, the periodic impact components in the signal can be effectively enhanced, which makes a good foundation for the feature extraction of fault signals.

In summary, this paper proposed a fault feature extraction method combining FDM-RobustICA and MOMEDA. Firstly, the FDM is used to decompose the vibration signal of the bearing and obtain several Fourier intrinsic band functions (FIBF). Then, by combining the cross-correlation analysis criterion and the kurtosis criterion, an effective FIBF component is selected as the observation signal, and blind source separation is performed. Thirdly, MOMEDA is used to enhance the periodic impact components in the noise-reduced signal. Finally, the Hilbert envelope demodulation is used to obtain the fault characteristic frequency, and the fault characteristic frequency is compared with the theoretical calculated value for fault diagnosis.

The structure of this paper is as follows. Section 2 introduces the basic principles of FDM, RobustICA, and MOMEDA. Section 3 briefly introduces the implementation details and fault feature extraction process of the method proposed in this paper. Section 4 uses the proposed method to analyze the simulation signal. Section 5 further verifies the effectiveness of the proposed method through the actual bearing fault signal. Section 6 gives the discussion and conclusion.

2. Theoretical Background

2.1. Fourier Decomposition Method. Fourier decomposition method (FDM) is a new type of the adaptive signal analysis method based on Fourier transform. This method first adaptively searches and analyzes the Fourier intrinsic band functions (FIBF) in the entire Fourier domain. Then, the nonlinear signal is adaptively decomposed into the sum of several physical Fourier intrinsic band functions (FIBF) and a residual component:

(1) FIBF has a zero mean value, namely, $\int_a^b y_i(t)\mathrm{d}t = 0$.

(2) Any two FIBF are orthogonal to each other, namely, $\int_a^b y_i(t)y_j(t)\mathrm{d}t = 0,\ i \neq j$.

(3) The analytic function form of FIBF has nonnegative instantaneous amplitude and frequency: $y_i(t)$ $\widehat{y}_j(t) = a_i(t)e^{j\varphi_i(t)}$, namely, $a_i(t) \geq 0$, $\varphi_i'(t) \geq 0$, $\forall t \in [a,b]$, and $y_i(t) \in C^{\infty}[a,b]$. Therefore, FIBF are the sum of zero-mean sine functions with continuous frequency bands.

Based on the definition of FIBF, the steps of the FDM are as follows:

Step 1: make a fast Fourier transformation of the signal $x(n)$, $X[k] = \mathrm{FFT}\{[x(n)]\}$.

Step 2: use forward search, which scans analytic Fourier intrinsic band functions (AFIBF) from low to high frequencies:

$$\mathrm{AFIBF} = \sum_{k=N_{i-1}+1}^{n} X[k]\sigma^{j2\pi kn/N} = a_i(n)e_X^{j\varphi_i[n]}. \quad (1)$$

In order to obtain the minimum number of AFIBF from low-frequency to high-frequency scanning, for each $i = 1, 2, \ldots, M$, start from $N_{i-1} + 1$ and gradually increase to reach the maximum N_i, where $N_0 = 0$ and $N_M = (N/2 - 1)$. It satisfies $N_{i-1} + 1 \leq N_{i-1} \leq (N/2 - 1)$ and also satisfies

$$a_i(t) \geq 0,\ \omega_i(t) = \frac{\varphi_i[n+1] - \varphi_i[n-1]}{2} \geq 0, \quad \forall t. \quad (2)$$

Similarly, a reverse search can also be performed, namely, scanning the AFIBF component from high to low frequencies. Correspondingly, change the upper and lower limits of the sum in equation (2) from N_i to $N_{i-1} - 1$, where $i = 1, 2, \ldots, M$, $N_0 = N/2$, and $N_M = 1$. The search should start from $N_{i-1} - 1$ and gradually decrease until the smallest N_i satisfies $1 \leq N_i \leq N_{i-1} - 1$, and the phase $\varphi_i[n]$ is a monotonically increasing function. The instantaneous frequency and amplitude can be calculated directly by AFIBF. Meanwhile, the real part of AFIBF is FIBF.

2.2. Robust Independent Component Analysis. Robust independent component analysis (RobustICA) is an independent component analysis algorithm based on kurtosis and optimal step size that has emerged in recent years on the basis of the original independent component analysis (ICA). The algorithm searches for the global optimal step size through the kurtosis comparison function, finds the demixing matrix, and calculates the approximate value of the source signal. The frame of independent component analysis is shown in Figure 1. The purpose of independent component analysis is to separate independent source signal components from the mixed signal.

Let n-dimensional random observation vectors conform to the following model:

$$x = AS + N, \quad (3)$$

where $S = [s_1, s_2 \ldots, s_m]^T$ and $x = [x_1, x_2 \ldots, x_n]^T$. S is the m-dimensional signal vector, which means that the number of mixed signals is m. N is the n-dimensional observation vector, which means that the number of mixed signals is n. A is an $n \times m$ matrix. The basic idea of ICA is to solve the separation matrix W and make an optimal estimate y of the source signal S when only the observation signal x is known:

$$y = Wx. \quad (4)$$

Compared with the traditional ICA, RobustICA does not need to prewhiten the data, which reduces the amount of calculation. At the same time, RobustICA can be used to process the sub-Gaussian signal and the super-Gaussian signal. When the Gaussian property of the signal is known, it can extract only the components of interest in the source signal without increasing the complexity of the operation and the estimation error. The linear search method used by RobustICA can ensure that the optimization can be achieved in all the processes of component separation. Assuming the output signal is $y = Wx$ (W is the $m \times n$-dimensional separation matrix), the kurtosis equation can be expressed as follows:

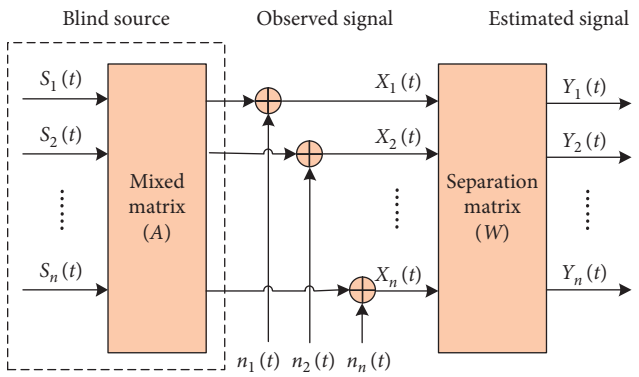

Figure 1: Frame of independent component analysis.

$$K(W) = \frac{E\{|y|^4\} - 2E^2\{|y|^2\} - |E\{y^2\}|^2}{E^2\{|y|^2\}}. \tag{5}$$

In the equation, $E\{\cdot\}$ represents the mathematical expectation. RobustICA directly uses the above equation as a comparison function without any simplification and then optimizes the kurtosis according to the strategy of the best linear optimization step size:

$$\mu_{\text{opt}} = \arg\max_u |K(W + \mu g)|, \tag{6}$$

where g is the search direction; usually, $g = \nabla_w K(W)$, which can be expressed as follows:

$$\nabla_w K(W) = \frac{4}{E^2\{|y|^2\}}\{E\{|y|^2\}yx - E\{yx\}\}E\{y^2\} - \frac{(E\{|y|^4\} - |E\{y^2\}|^2)E\{yx\}}{E\{|y|^2\}}. \tag{7}$$

In the process of iteration, the optimization method of RobustICA can be described as follows:

(1) Find the coefficients of the OS polynomial. When the kurtosis becomes a comparison function, the OS polynomial can be expressed as follows:

$$P(u) = \sum_{k=0}^{4} a_k u^k. \tag{8}$$

(2) Extract the root a of the OS polynomial $\{u^k\}_{k=1}^4$.

(3) Select the root that can make the best optimization step $\mu_{\text{opt}} = \arg\max_u |K(W + \mu g)|$ and take the largest value from the direction of iteration.

(4) Update μ_{opt} based on the value of the updated step W^+: $W^+ = W + \mu_{\text{opt}} g$.

(5) Normalize W^+: $W^+ \longleftarrow W^+/\|W^+\|$.

(6) Determine whether the iterative operation converges and meets the termination conditions. If it is not satisfied, then return to Step (1).

2.3. Multipoint Optimal Minimum Entropy Deconvolution Adjusted. If x is the vibration signal, y is the shock sequence. Meanwhile, h is the system frequency response function. e is the noise signal. The symbol $*$ is the multiplication symbol. The collected signal can be expressed as

$$x = h * y + e. \tag{9}$$

The essence of the MOMEDA is to use a noniterative method to find an optimal FIR filter. Recover the vibration shock signal from the output signal as much as possible through the deconvolution process, and reduce the impact of noise. The deconvolution process is as follows:

$$y = f * x = \sum_{k=1}^{N-L} f_k x_{k+L-1}, \tag{10}$$

where $k = 1, 2, \cdots, N - L$. According to the characteristics of the periodic shock signal, multipoint D-norm is introduced, namely,

$$\text{MDN}(y, t) = \frac{1}{\|t\|}\frac{t^T y}{\|y\|}, \tag{11}$$

$$\text{MOMEDA} = \max_f \text{MDN}(y, t) = \max_f \frac{t^{\text{T}} y}{\|y\|}. \tag{12}$$

In equation (12), t is a constant vector for determining the position and weight of the target impact component. The optimal filter f is obtained by solving the maximum value of the multipoint D-norm. At this time, the deconvolution process also obtains the optimal solution. In order to find the extreme value of equation (12), the filter coefficient $f = (f_1, f_2, \cdots, f_L)$ is first derived.

$$\frac{\text{d}}{\text{d}f}\left(\frac{t^T y}{\|y\|}\right) = \frac{\text{d}}{\text{d}f}\frac{t_1 y_1}{\|y\|} + \frac{\text{d}}{\text{d}f}\frac{t_2 y_2}{\|y\|} + \cdots + \frac{\text{d}}{\text{d}f}\frac{t_{N-L} y_{N-L}}{\|y\|}, \tag{13}$$

$$\frac{\text{d}}{\text{d}f}\frac{t_k y_k}{\|y\|} = \|y\|^{-1} t_k M_k - \|y\|^{-3} t_k y_k X_0 y, \tag{14}$$

$$M_k = [x_{x+L-1}, x_{x+L-2}, \cdots, x_k]^T. \tag{15}$$

Therefore, equation (13) can be written as follows:

$$\frac{\text{d}}{\text{d}f}\left(\frac{t^T y}{\|y\|}\right) = \|y\|^{-1}(t_1 M_1 + t_2 M_2 + \cdots t_{N-L} M_{N-L}) - \|y\|^{-3} t^T y X_0 y. \tag{16}$$

Let $X_0 = [M_1, M_1, \cdots, M_k]$ in the above equation; then, equation (13) is equivalent to the following equation:

$$\|y\|^{-1} X_0 t - \|y\|^{-3} t^T y X_0 y = 0. \tag{17}$$

By sorting out the above equation, we can get

$$\frac{t^T y}{\|y\|^{-2}} X_0 y = X_0 t. \tag{18}$$

Since $y = X_0^T f$, if $(X_0 X_0^T)^{-1}$ exists, the following equation can be obtained:

$$\left(\frac{t^T y}{\|y\|^2}\right) X_0 f = \left(X_0 X_0^T\right)^{-1} X_0 t. \tag{19}$$

The special solution of the above equation is a set of optimal filters, as shown in the following equation:

$$f = \left(X_0 X_0^T\right)^{-1} X_0 t. \tag{20}$$

Substituting the above equation into $y = X_0^T f$, the original impact signal y can be reconstructed.

3. The Process of Fault Feature Extraction

Although the adaptive decomposition of component signals by the FDM avoids modal overlapping and endpoint effect, the blind selection and rejection of component signals only by the FDM may lead to incomplete extraction of fault feature information. RobustICA, as a newer method in blind source separation, is not easily interfered by strong noise. However, the processed bearing vibration signal is often a single channel, which does not meet the conditions of use of RobustICA. To a great extent, it restricts the application of this kind of algorithm. Therefore, in order to give full play to the advantages of FDM and RobustICA in signal processing, this study used a combination of FDM and RobustICA to reduce noise on bearing fault signals. When the original bearing fault signal with noise is decomposed by the FDM, a number of FIBF components from high to low frequency will be obtained. Under actual working conditions, the noise signal is unknown, which brings great difficulties to the construction of the virtual noise channel. If the method of constructing the virtual noise channel is inappropriate, it will directly affect the effect of signal noise reduction. Considering the particularity of mechanical signals, this research will judge the sensitivity of each component signal to interference noise and fault impact by combining cross-correlation analysis criteria and kurtosis criteria, so as to build a virtual noise channel.

According to the definition of the cross-correlation criterion, the correlation coefficient can be used as an index to evaluate the degree of correlation between two signals. The larger the correlation coefficient value, the higher the correlation with the original signal. By using this criterion, the degree of correlation between each component signal obtained from the decomposition and the original signal can be known. The calculation method of the correlation number is as follows:

$$r = \frac{\sum_{i=0}^{n} (x_i - \overline{x})(y_i - \overline{y})}{\sqrt{\sum_{i=0}^{n} (x_i - \overline{x})^2 (y_i - \overline{y})^2}}, \tag{21}$$

where x_i and $\overline{x}$ are specific values and average values of the signal x. At the same time, y_i and $\overline{y}$ are specific values and average values of the signal y, respectively.

Kurtosis can be used to measure the peak degree of signal waveform, and it is more sensitive to the impact components in the signal. The higher the proportion of impact components is, the higher the kurtosis value will be. For bearings, the kurtosis value is close to the normal distribution under normal operation, and it will increase significantly when faults occur. The calculation method is as follows:

$$K_i = \frac{1}{n} \sum_{i=1}^{n} \left(\frac{x_i - \overline{x}}{\sigma}\right)^4, \tag{22}$$

where x_i and $\overline{x}$ are specific values and average values of the signal x, σ is the standard deviation of the signal, and n is the number of samples.

After finding the correlation coefficient and kurtosis value of each FIBF component through the above criteria, the virtual channel is further constructed based on this. Then, RobustICA is used to recover the independent component of the effective signal and the independent component mainly of noise. Under the strong noise interference, the fault feature of the separated effective signal is still weak. In order to enhance the impact component of the bearing fault signal after noise reduction, this research introduced the MOMEDA to filter the signal and finally calculated the Hilbert envelope spectrum of the filtered signal and extracted the corresponding fault frequency, so as to accurately diagnose the fault. The flowchart of the proposed method is shown in Figure 2.

The specific steps are as follows:

(1) FDM method is used to decompose the vibration signals of the rolling bearing under different fault conditions, and several FIBF components with high frequency and low frequency are obtained.

(2) According to the cross-correlation and kurtosis criteria, the cross-correlation coefficient and kurtosis value of each FIBF component are calculated. Then, the signal component is selected that is highly correlated with the original signal and has a large impact component ratio (the signal components with cross-correlation coefficient greater than 0.3 and kurtosis value greater than 3 are selected in this research) to construct an observation signal channel. At the same time, the remaining signal components are used to construct a virtual noise signal channel.

(3) The observation signal and the virtual noise signal are used as the input matrix of the blind source separation, and then the signal is demixed by using RobustICA to achieve the noise reduction of the vibration signal.

(4) The MOMEDA is used to enhance the periodic impact component of the noise reduced signal.

(5) The signal obtained in the previous step is demodulated by Hilbert envelope, and then the fault frequency is extracted for fault diagnosis.

4. Simulations and Comparative Analysis

In order to verify the effectiveness of the method proposed in this paper, the fault signal of the rolling bearing is simulated and analyzed. The structure of the analog signal is as follows:

$$s(t) = y_0 e^{-2\pi f_n \xi t} \sin\left(2\pi f_n \sqrt{1 - \xi^2}\, t\right), \tag{23}$$

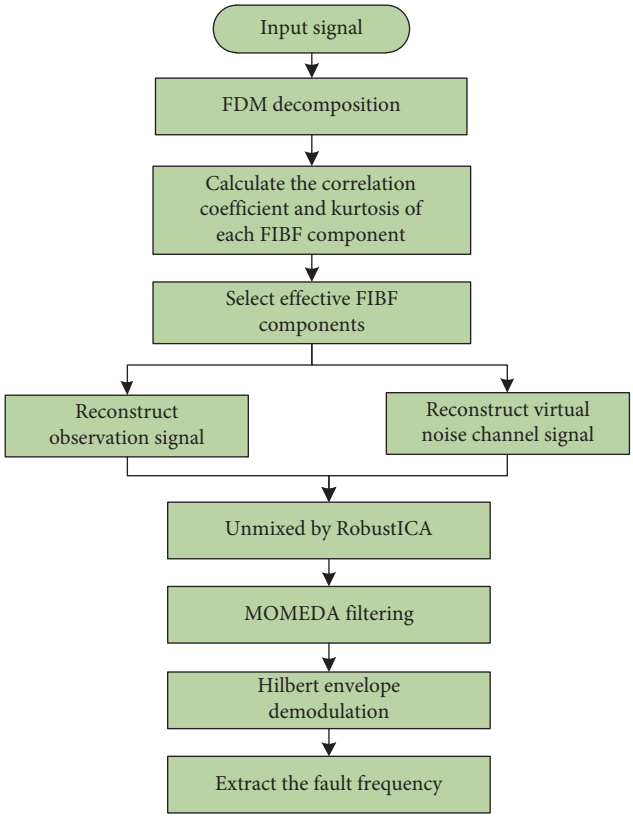

Figure 2: The flowchart of the proposed method.

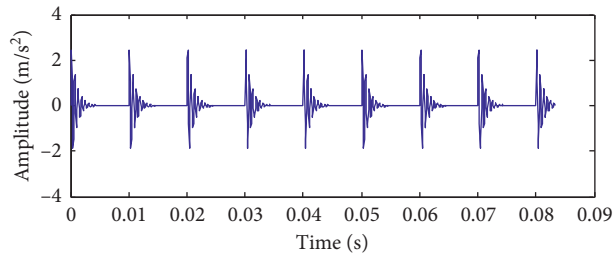

Figure 3: Original signal.

where the natural frequency of the bearing f_n is 3000 Hz, the displacement constant y_0 is 5, the damping coefficient ξ is 1, the period of the impact failure is 0.01 s, the sampling frequency f_s is 12 kHz, and the number of sampling points N is 1000. Through calculation, the fault frequency f_0 is 100 Hz. The time-domain waveform of the original signal s (t) is shown in Figure 3. After the Gaussian white noise with a signal-to-noise ratio of −5 dB is added to the original signal s (t), the time-domain waveform and frequency-domain waveform of the mixed signal y (t) are shown in Figure 4. It can be seen from Figure 4 that the impact characteristics of the bearing have been completely annihilated due to the interference of noise, and the impact interval of the bearing cannot be distinguished from the figure.

Next, the fault feature extraction method proposed in the paper is used to process and analyze the above analog fault signals. Firstly, the FDM is performed on the mixed signal y (t), and Figure 5 shows the results of the decomposition. In order to highlight the advantages of the method proposed in this paper, the LMD and ITD, commonly used in the field of fault diagnosis, are used to decompose the signal, and further analysis is carried out. The decomposition results of the above two methods can be seen in Figure 6. As shown in Figure 5, the mixed signal y (t) is decomposed into 19 Fourier intrinsic band functions (FIBF) from high to low frequencies. Because FDM overcomes the problems of modal aliasing and endpoint effects to a certain extent and has a strict theoretical basis, the components obtained by the decomposition clearly reflect the local characteristic information of the original signal.

In order to select the signal components that meet the conditions from the decomposition results, the correlation coefficient C (t) and the kurtosis value K (t) of each component signal are calculated. As can be seen from Table 1, only the kurtosis values of the y_9, y_{11}, and y_{12} components are greater than 3, and their correlation values are greater than 0.3, indicating that the above component signals have a high correlation with the original signals and contain more impact components. Therefore, the above three components are selected to reconstruct the observation signal channel, and the remaining signal components are used to reconstruct the noise signal channel. At the same time, the calculation results of the correlation and kurtosis of the signal components based on the LMD and ITD are shown in Tables 2 and 3, respectively. It can be seen that the correlation and kurtosis values of the PF1 and PF2 components in Table 2 and the PRC2 and PRC3 components in Table 3 meet the set threshold conditions. Therefore, the above component signals are selected to reconstruct the observation signals, and the remaining component signals are used to reconstruct the noise signal channel. Then, they are separately demixed by the RobustICA to achieve the separation of the signal and noise. The noise reduction results based on FDM-RobustICA, LMD-RobustICA, and ITD-RobustICA are shown in Figures 7–9, respectively.

By comparing the signal and noise separation results in Figures 7–9, it can be seen that the impact components in the target signal after noise reduction by FDM-RobustICA are more obvious, which can better extract useful information from noise-containing signals and weaken the influence of strong background noise. However, the time-domain waveform of the target signal based on LMD-RobustICA and ITD-RobustICA noise reduction methods is different from that of the original signal to some extent. Meanwhile, because there is no prior information of the fault in the process of using the RobustICA to carry out the demixing operation, the system has uncertainty and the signal amplitude after demixing changes to varying degrees but does not affect the noise reduction analysis.

In order to quantitatively analyze the noise reduction effect based on the above three methods, kurtosis value, correlation number, and noise reduction time are selected as the evaluation indexes. The larger the kurtosis value is, the more fault information in the signal is. The larger the correlation number is, the more complete the effective

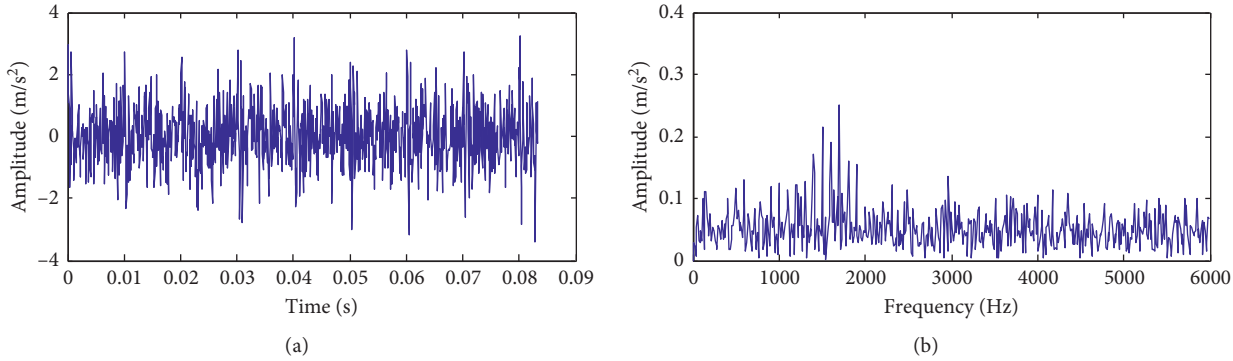

Figure 4: (a) Time-domain analysis and (b) frequency-domain analysis of the mixed signal with SNR = −5 dB.

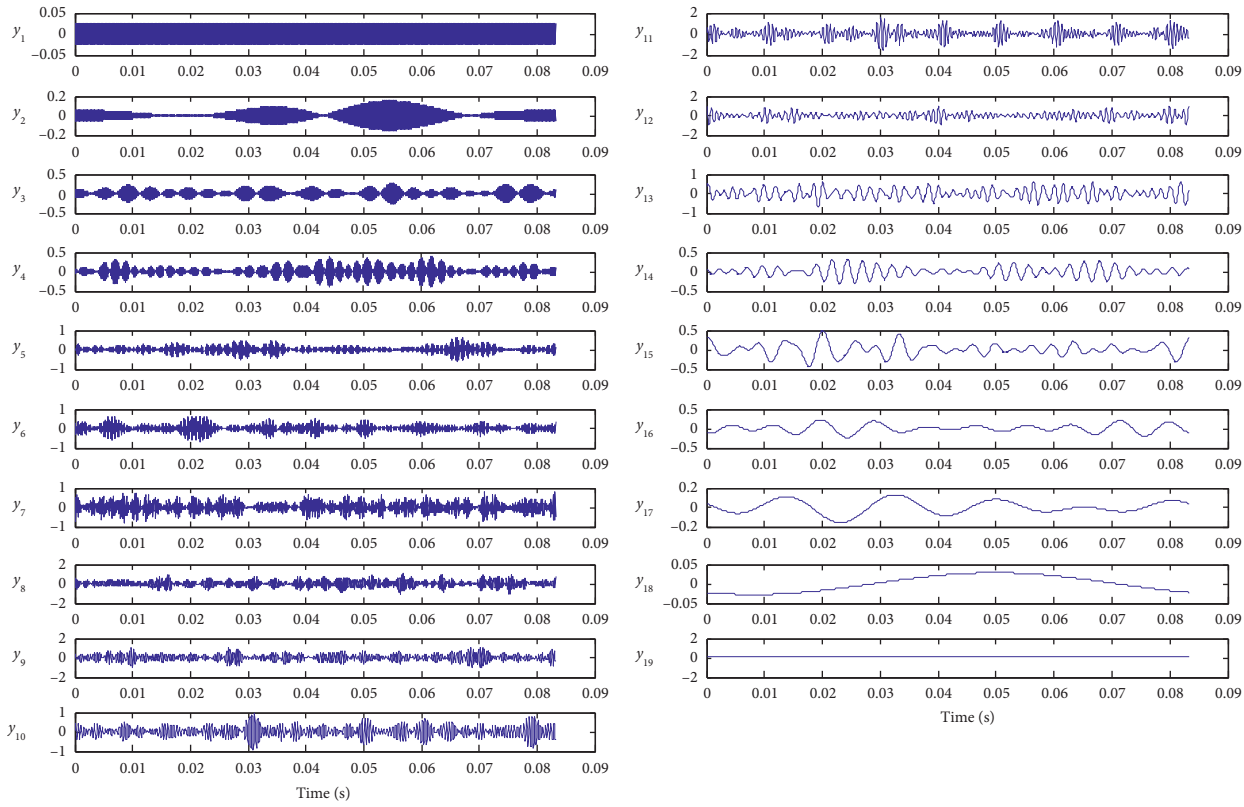

Figure 5: The decomposition result by the FDM.

information of the signal is retained. The shorter the noise reduction time is, the higher the operation efficiency of the algorithm is. The calculation results are shown in Table 4. It can be seen from Table 4 that the correlation value and kurtosis value of the noise reduced signal based on FDM-RobustICA are the largest, which shows that the noise reduced signal obtained by the method proposed has a high similarity with the original signal. At the same time, this method not only reduces the noise interference but also retains the fault characteristic information well. Although there is a certain gap in noise reduction time between ITD-RobustICA and FDM-RobustICA, it is not significant.

In order to further compare the effects of the above three methods on the separation of the target signal and noise, the signals obtained by the above three methods are separately demodulated by Hilbert envelope, and then the corresponding envelope spectrum is obtained. The results are shown in Figures 10–12. It can be seen from Figure 11 that the envelope spectrum of the noise signal separated by LMD-RobustICA has components such as one to four doubling fault frequencies, and the fault frequency amplitude is relatively high. It can be seen from Figure 12 that the envelope spectrum of the noise signal obtained by ITD-RobustICA also contains the components of one, two, and three doubling fault frequencies. It shows that, after the above two methods are processed, the target signal and noise have not been completely separated, and some of the fault signals are missing from the separated target signal. It can be seen from

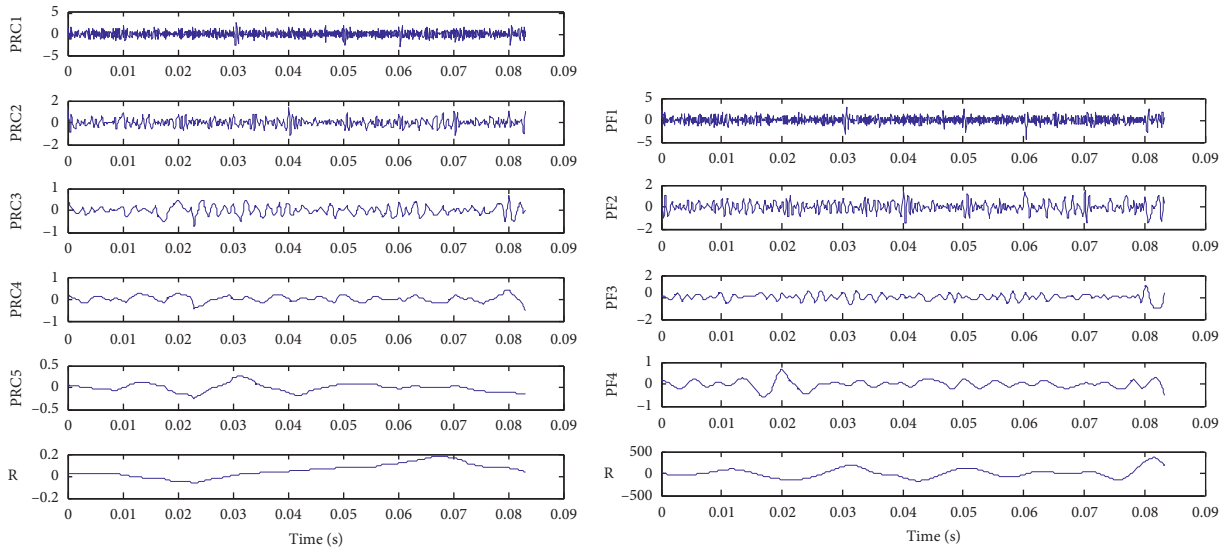

(a) (b)

Figure 6: Signal decomposition results. (a) The decomposition result by ITD. (b) The decomposition result by LMD.

Table 1: The correlation coefficient and kurtosis between the FIBF and the original signal.

	y_1	y_2	y_3	y_4	y_5	y_6	y_7	y_8	y_9	y_{10}	y_{11}	y_{12}	y_{13}	y_{14}	y_{15}	y_{16}	y_{17}	y_{18}	y_{19}
$C(t)$	0.026	0.073	0.121	0.154	0.194	0.221	0.313	0.363	0.351	0.283	0.445	0.326	0.268	0.127	0.164	0.104	0.070	0.021	0.000
$K(t)$	1.000	2.681	2.166	2.783	3.303	3.508	2.531	2.924	3.348	3.405	4.246	3.380	2.376	2.955	3.604	2.637	2.562	1.500	1.000

Table 2: The correlation coefficient and kurtosis between the PF and the original signal.

	PF1	PF2	PF3	PF4
$C(t)$	0.804	0.467	0.211	0.149
$K(t)$	3.825	3.608	4.864	4.982

Table 3: The correlation coefficient and kurtosis between the PRC and the original signal.

	PRC1	PRC2	PRC3	PRC4	PRC5
$C(t)$	0.866	0.584	0.333	0.180	0.075
$K(t)$	2.929	3.768	3.121	3.692	3.312

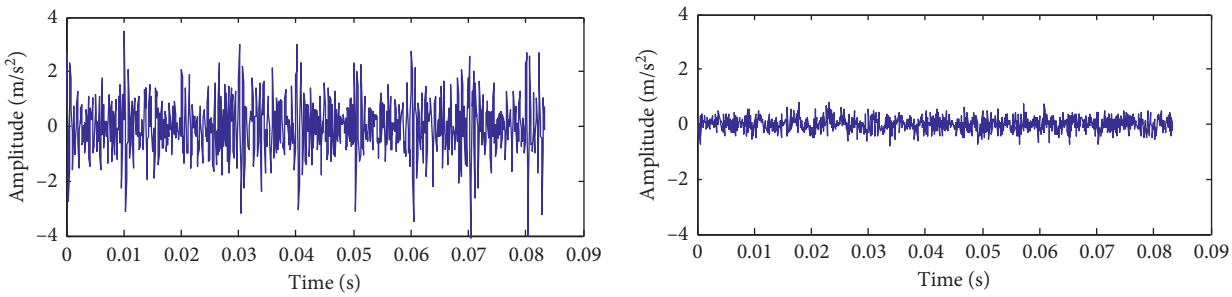

(a) (b)

Figure 7: The waveform of each independent component by the FDM-RobustICA method. (a) The waveform of the target signal. (b) The waveform of the noise signal.

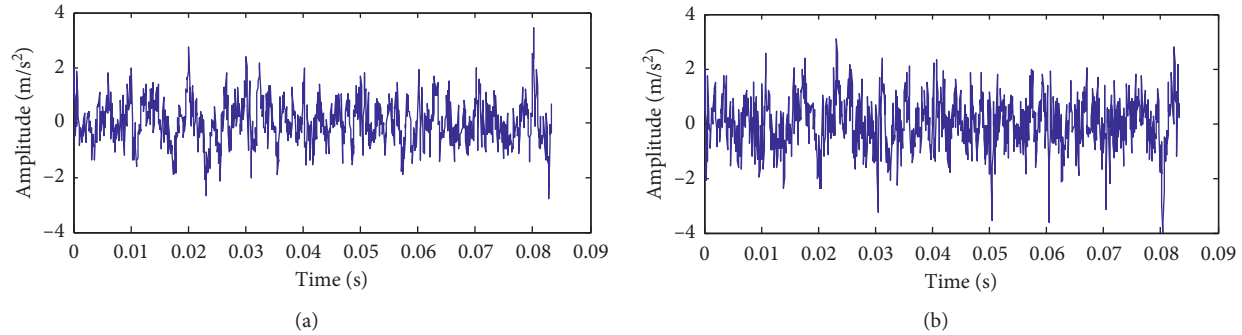

Figure 8: The waveform of each independent component by the LMD-RobustICA method. (a) The waveform of the target signal. (b) The waveform of the noise signal.

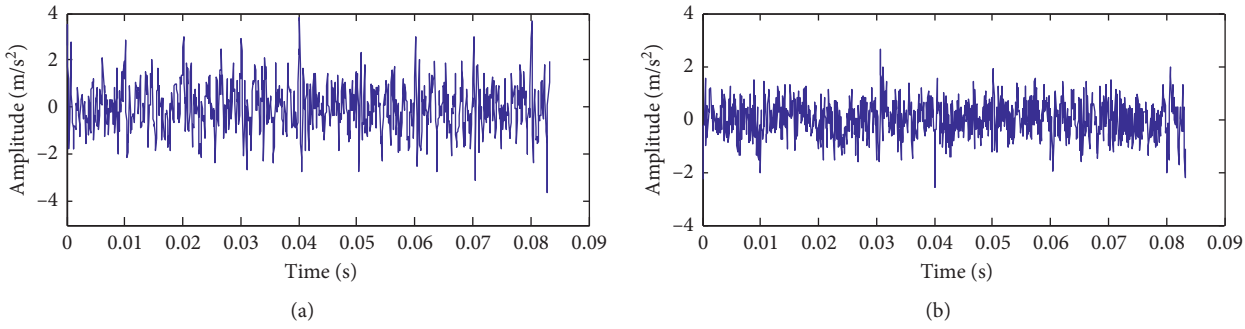

Figure 9: The waveform of each independent component by the ITD-RobustICA method. (a) The waveform of the target signal. (b) The waveform of the noise signal.

Table 4: Comparison of noise reduction results of different methods.

Evaluation index	FDM-RobustICA	LMD-RobustICA	ITD-RobustICA
Kurtosis and correlation coefficient	3.907 0.582	3.602 0.374	3.630 0.480
Noise reduction time	1.378	0.0889	0.103

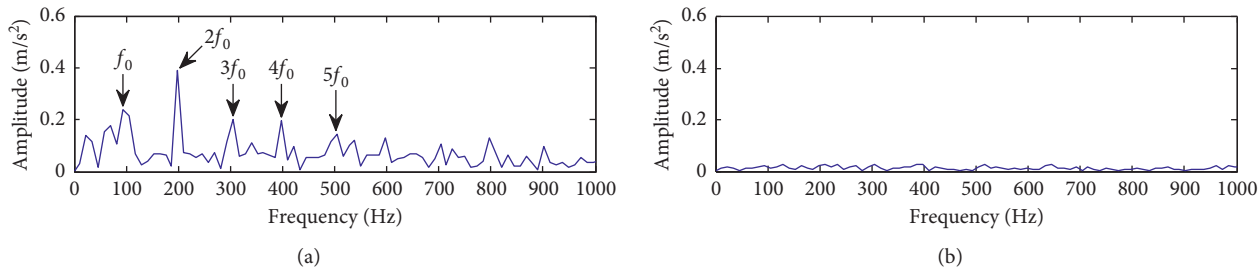

Figure 10: The envelope analysis of each independent component by the FDM-RobustICA method. (a) The envelope analysis of the target signal. (b) The envelope analysis of the noise signal.

Figure 10 that the amplitude of the fault characteristic frequency in the envelope spectrum of the target signal has been increased to a certain extent. Meanwhile, the fault characteristic frequency and its doubling frequency can be obtained. In addition, there is no fault information in the envelope spectrum of the noise signal in Figure 10, indicating that the fault signal and the noise signal are effectively separated. However, some irrelevant frequency components still appear in the envelope spectrum of the fault signal, which have a certain degree of interference to fault diagnosis.

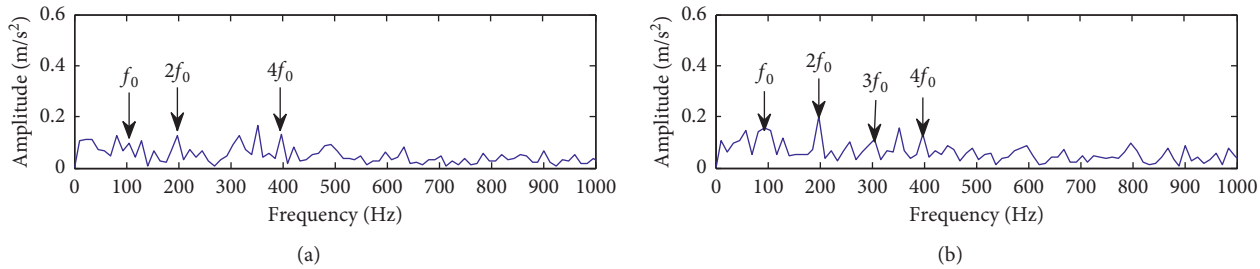

Figure 11: The envelope analysis of each independent component by the LMD-RobustICA method. (a) The envelope analysis of the target signal. (b) The envelope analysis of the noise signal.

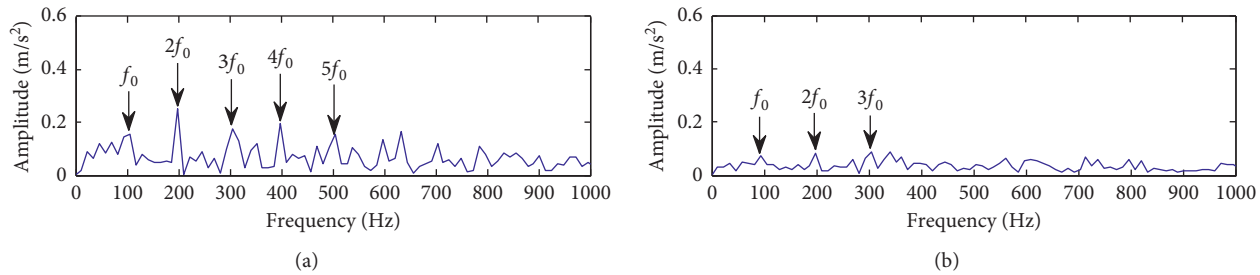

Figure 12: The envelope analysis of each independent component by the ITD-RobustICA method. (a) The envelope analysis of the target signal. (b) The envelope analysis of the noise signal.

Therefore, it is necessary to further enhance the periodic impact component of the noise reduced signal through MOMEDA filtering.

Next, the experiment uses MOMEDA to enhance the signal after FDM-RobustICA noise reduction, and then the signal is demodulated by Hilbert envelope. Figure 13 shows the time-domain waveform and envelope spectra of the MOMEDA filter signal. It can be seen from Figure 13 that the periodic impact component is very obvious after filtering by MOMEDA. There are more prominent fault features in the envelope spectrum, and there are large peaks at the frequencies of 105.5 Hz, 199.2 Hz, 304.7 Hz, 398.4 Hz, 503.9 Hz, 597.7 Hz, 703.1 Hz, 796.9 Hz, 902.3 Hz, and so on. The above peaks are very close to the simulated fault characteristic frequency of 100 Hz and the doubling frequency from two to ten. At the same time, the amplitudes of other noninteger multiples at the characteristic frequency of the fault are basically close to 0, indicating that the signal components unrelated to the fault impact have been greatly weakened. Therefore, the bearing fault can be accurately diagnosed according to the characteristic frequency.

5. Application to Roller Bearing Testing

In order to further verify the effectiveness of the method proposed in this paper, the bearing data of CWRU are used for analysis [38]. The model of the rolling bearing at the drive end of the motor is 6205-2RSJEMSKF, and the motor speed is 1797 rpm (namely, the rotation frequency is 1797/60 Hz = 29.95 Hz). The sampling frequency of the fault signal is 12 kHz, and the length of experimental data is 2048. The specific technical parameters are shown in Table 5.

Outer race defect frequency:

$$\mathrm{BPFO} = \frac{Z}{2}\left(1 - \frac{d}{D}\cos\alpha\right) \times f_r. \tag{24}$$

Inner race defect frequency:

$$\mathrm{BPFI} = \frac{Z}{2}\left(1 + \frac{d}{D}\cos\alpha\right) \times f_r. \tag{25}$$

Rolling element frequency:

$$\mathrm{BPFR} = \frac{D}{2d}\left(1 - \left(\frac{d}{D}\right)^2 \cos^2\alpha\right) \times f_r, \tag{26}$$

where Z is the number of rolling elements, d is the rolling element diameter, D is the bearing pitch diameter, α is the contact angle, and f_r is the shaft rotation frequency (Hz).

Based on the bearing parameters shown in Table 5 and equations (24)–(26), the fault characteristic frequency of the rolling bearing, BPFO = 107.36 Hz, BPFI = 162.19 Hz, and BPFR = 141.1693 Hz, is calculated, respectively in Table 6 [39].

5.1. Inner Ring Signal Analysis of CWRU Bearings. The time domain and the frequency domain of the bearing inner ring fault signal are shown in Figure 14. Although it is disturbed by noise to some extent, some periodic pulses can still be seen. To test the effectiveness of the proposed method under strong noise interference, Gaussian white noise with a signal-to-noise ratio of −5 dB is added to the original inner ring fault signal in this research. The time domain and the frequency domain of the generated mixed signal are shown

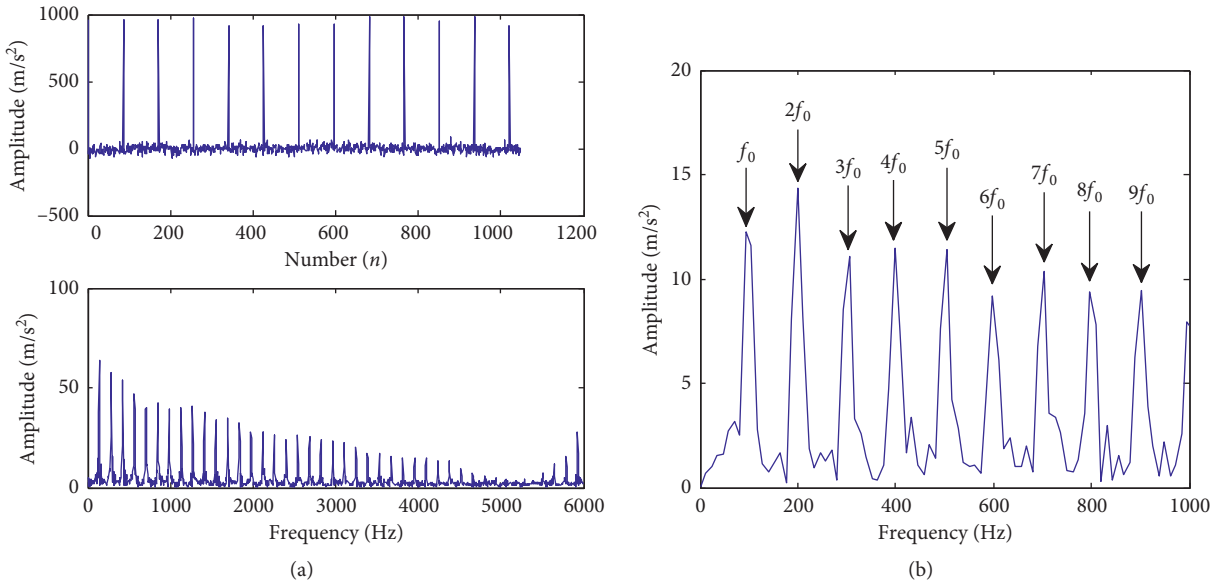

Figure 13: The MOMEDA filter signal and its envelope spectrum. (a) Time-domain waveform and envelope spectrum of the MOMEDA filter signal. (b) Part band envelope spectrum of the MOMEDA filter signal.

Table 5: The bearing technical parameters of SKF 6205.

Rolling element number (Z)	Inner diameter (inches)	Outer diameter (inches)	Rolling element diameter d (inches)	Contact angle (α)	Pitch circle diameter D (inches)	Speed (rpm)
9	0.9843	2.0472	0.3126	0^0	1.5327	1797

Table 6: Fault characteristic frequency (unit: Hz).

Inner ring fault	Outer ring fault	Rolling element fault
162.1852	107.3648	141.1693

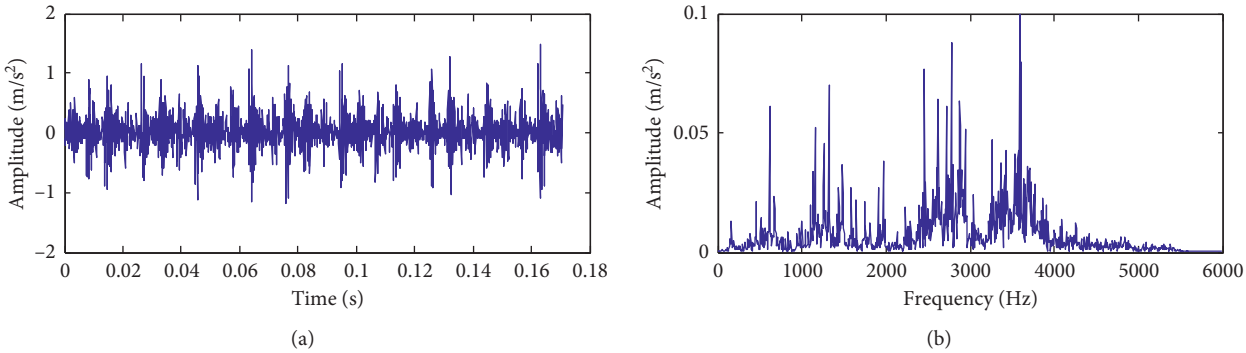

Figure 14: (a) Time-domain analysis and (b) frequency-domain analysis of the original inner ring fault signal.

in Figure 15. Due to the enhancement of noise interference, it is impossible to distinguish the periodic pulse features from Figure 15, and it is difficult to extract the fault feature frequency directly from the time domain and the frequency domain.

Next, the method proposed in this paper is used to process the mixed signal of the inner ring with added noise. After the mixed signal is decomposed by the FDM, 25 FIBF components are obtained, and the decomposition results are shown in Figure 16. Due to the limited length of the article, only the first 20 FIBF components are listed in it. Then, the cross-correlation coefficient and kurtosis value of each signal component are calculated, and the results are shown in Table 7. It can be seen from Table 7 that the signal components of y_{10}, y_{11}, and y_{12} meet the set threshold conditions, indicating that they have a high degree of correlation with the original signal and retain a lot of impact features in the

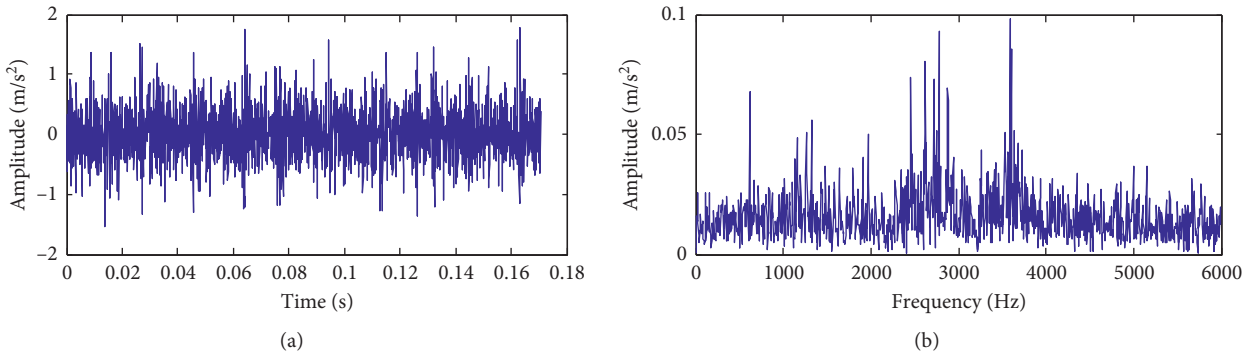

Figure 15: (a) Time-domain analysis and (b) frequency-domain analysis of the mixed signal with SNR = −5 dB.

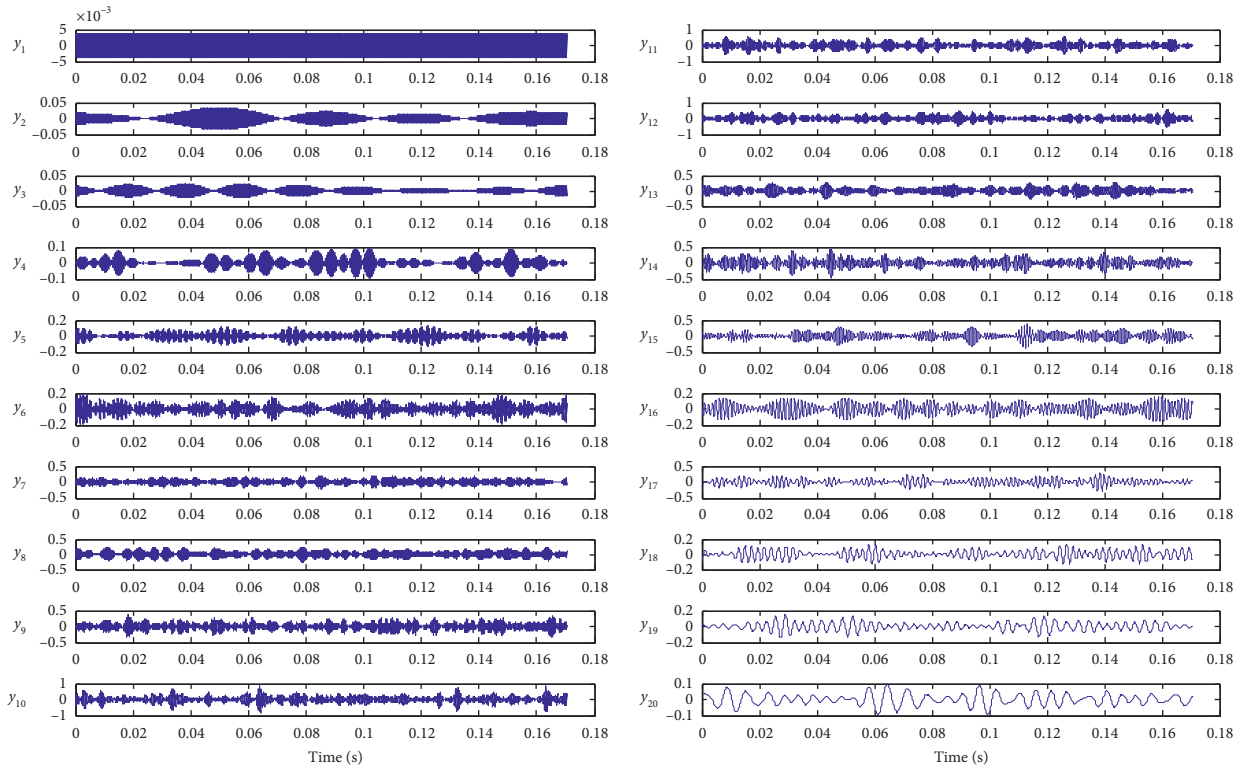

Figure 16: FDM decomposition result.

original signal. Therefore, the above three signal components are extracted to construct the target signal channel, and the remaining components are reconstructed as the virtual noise channel. The blind source separation is performed by RobustICA, and two sets of independent component time-domain waveforms are obtained. The results are shown in Figure 17.

It can be seen from Figure 17 that, after the noise reduction of RobustICA, the noise and the target signal are separated. In order to further compare the effect of noise reduction, the separated target signal and the mixed signal with −5 dB noise added were analyzed by the Hilbert envelope spectrum, respectively. The results are shown in Figure 18. By analyzing Figure 18, it can be known that, before noise reduction, the amplitude of the envelope spectrum of the fault signal is very low due to the influence of noise, and the interference of irrelevant frequency components on the fault diagnosis is large. Although the fault frequency of the inner ring can be found, as well as 2 doubling frequency, 5 doubling frequency, etc., the amplitude is low, and it is hard to recognize. After the noise reduction by RobustICA, the envelope spectrum amplitude of the obtained target signal has been greatly improved, and the fault characteristics are more prominent. At the same time, there were large peaks at frequencies of 164.1 Hz, 322.3 Hz, 486.3 Hz, 644.5 Hz, 808.6 Hz, 972.7 Hz, and so on. The above peak values are very close to the theoretical calculated value of the fault characteristic frequency of the bearing inner ring of 162.1852 Hz and the 2–6 doubling frequency. However, there are also many peaks in the

Table 7: The correlation coefficient and kurtosis between the FIBF and the original signal.

	y_1	y_2	y_3	y_4	y_5	y_6	y_7	y_8	y_9	y_{10}	y_{11}	y_{12}	y_{13}	y_{14}	y_{15}	y_{16}	y_{17}	y_{18}	y_{19}	y_{20}	y_{21}	y_{22}	y_{23}	y_{24}	y_{25}
$C(t)$	0.008	0.041	0.028	0.082	0.115	0.149	0.181	0.211	0.259	0.468	0.430	0.360	0.215	0.270	0.234	0.143	0.202	0.117	0.114	0.082	0.060	0.036	0.059	0.026	0.00
$K(t)$	1.000	1.958	1.928	3.032	2.501	2.708	2.375	2.470	2.847	4.302	3.221	3.183	2.793	3.417	3.383	2.424	2.881	2.620	3.039	2.866	2.444	2.743	2.073	1.500	1.000

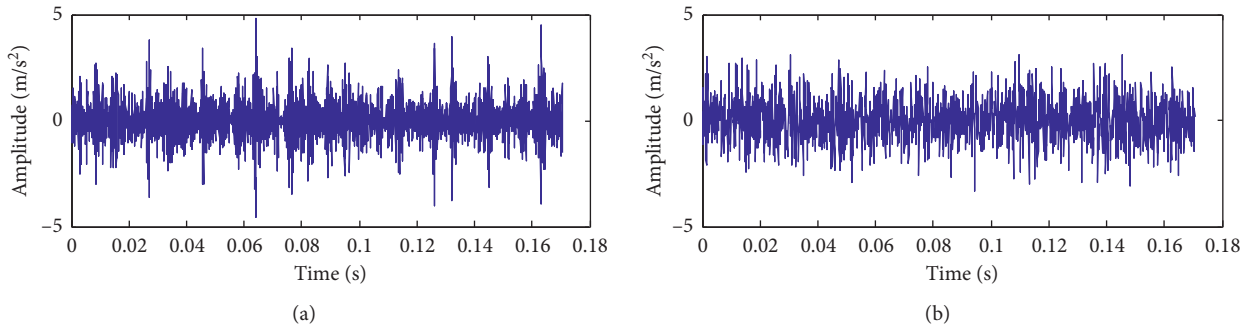

Figure 17: The waveform of each independent component. (a) The waveform of the target signal. (b) The waveform of the noise signal.

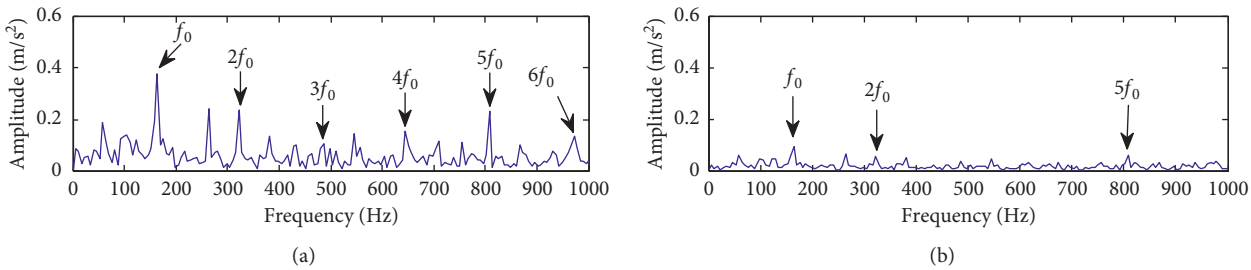

Figure 18: Envelope spectrum analysis. (a) Envelope spectrum analysis of the target signal denoised by FDM-RobustICA. (b) Envelope spectrum of the mixed signal.

envelope spectrum of the signal that have nothing to do with the characteristic frequency of the fault, and these peaks will affect the results of fault diagnosis. Therefore, the periodic impact components in the signal after noise reduction will be further extracted by MOMEDA filtering, and the extraction results are shown in Figure 19.

It can be clearly seen from Figure 19 that the MOMEDA has effectively extracted the periodic fault shock components in the reconstructed signal, and a larger peak has appeared. Meanwhile, the signal components unrelated to the fault shock have been weakened. By comparing the envelope spectrum of the signals in Figures 19 and 18, it can be seen that, after MOMEDA filtering, the characteristic frequency of the fault is more obvious. Not only the fault frequency of the bearing inner ring (164.1 Hz) can be clearly distinguished but also the 2 doubling frequency (322.3 Hz), 3 doubling frequency (486.3 Hz), 4 doubling frequency (644.5 Hz), 5 doubling frequency (808.6 Hz), and so on, are all clearly visible, and they are very close to the theoretically calculated fault characteristic frequency and doubling frequency. Therefore, the fault of bearing inner ring can be accurately diagnosed according to fault characteristic frequency.

5.2. Outer Ring Signal Analysis of CWRU Bearings. The time domain and the frequency domain of the bearing outer ring fault signal are shown in Figure 20, from which the periodic pulse characteristics can be seen. After adding Gaussian white noise with a signal-to-noise ratio of −5 dB to the outer ring fault signal, the time domain and the frequency domain of the generated mixed signal are shown in Figure 21. Due to the interference of noise, it is difficult to extract the fault feature frequency.

Then, the method proposed in this paper is used to process the mixed signal of the outer ring with added noise. After FDM decomposition, 25 FIBF components are obtained. The decomposition results are shown in Figure 22. Due to the limitation of the length of the article, only the first 20 FIBF components are listed in the figure. By calculating the cross-correlation coefficient and kurtosis value of each signal component, the results are shown in Table 8. After comparing the data results in Table 8, it can be seen that the signal component of y_{12} meets the threshold conditions. Therefore, the above signal component is extracted to reconstruct the target signal channel, and the remaining components are reconstructed as the virtual noise channel. Through the RobustICA for blind source separation, the time-domain waveforms of two groups of independent components are obtained, and the results are shown in Figure 23.

After comparing Figures 23 and 21, it can be seen that most of the noise is effectively filtered out through blind source separation processing, and the waveform of the target signal is highly similar to the original outer ring fault signal without the noise added. In order to further compare the noise reduction effect, Hilbert envelope spectrum analysis is carried out for the target signal obtained by separation and the mixed signal with −5 dB noise added. The results are shown in Figure 24. Through the analysis of Figure 24, it can be seen that, in the envelope spectrum of the outer ring fault signal without noise reduction, only the frequencies of 105.5 Hz and 216.8 Hz have relatively high peaks, which are

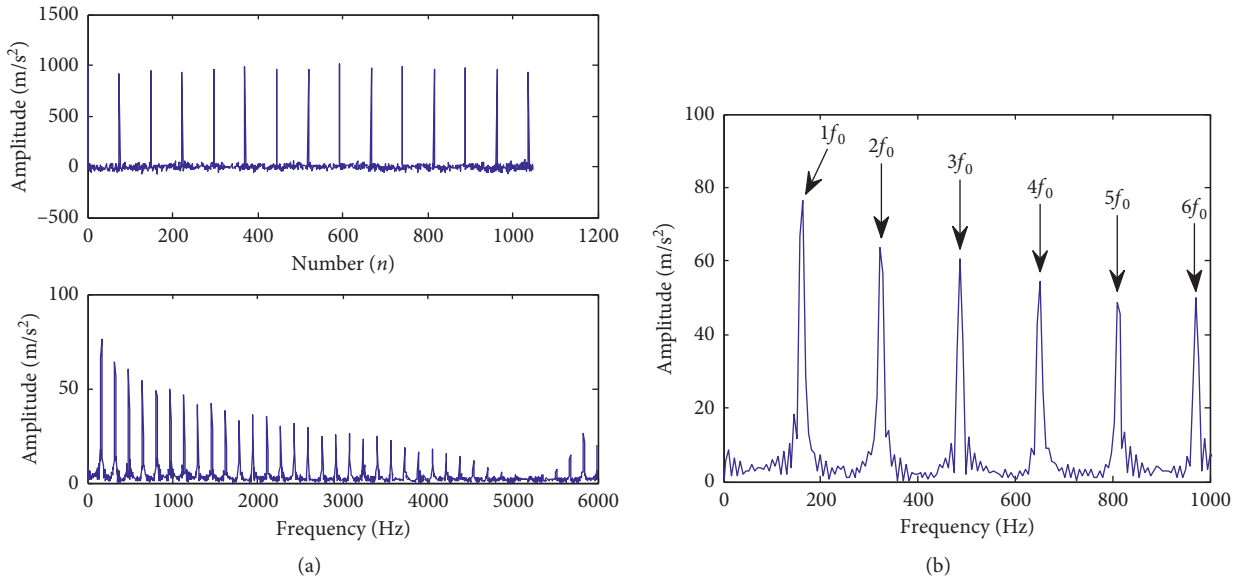

Figure 19: The inner ring MOMEDA filter signal and its envelope spectrum. (a) Time-domain waveform and the envelope spectrum of the MOMEDA filter signal. (b) Part band envelope spectrum of the MOMEDA filter signal.

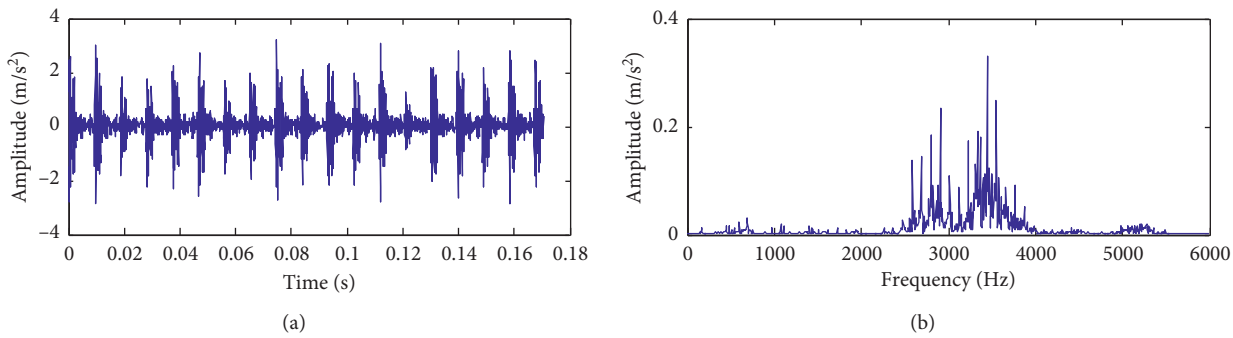

Figure 20: (a) Time-domain analysis and (b) frequency-domain analysis of the original outer ring fault signal.

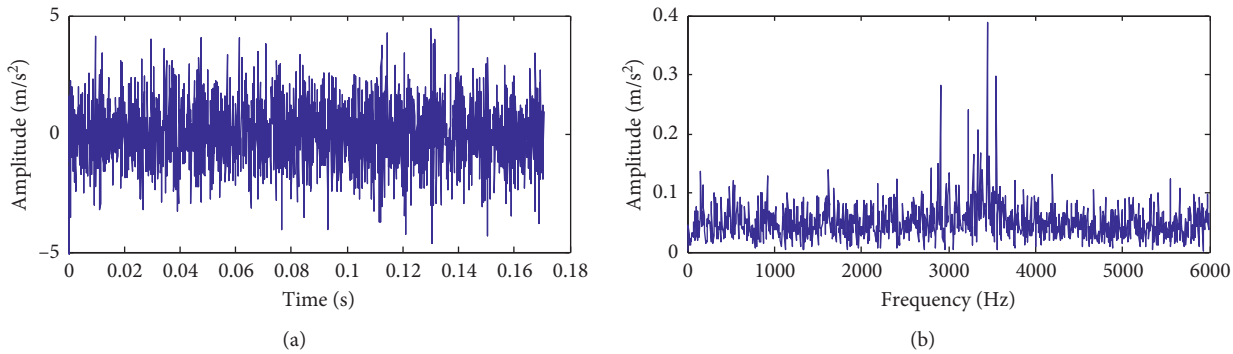

Figure 21: (a) Time-domain analysis and (b) frequency-domain analysis of the mixed signal with SNR = −5 dB.

very close to the theoretical calculation value of 107.3648 Hz of the bearing outer ring fault characteristic frequency and the double frequency of the basic fault frequency. After noise reduction by RobustICA, there are three peaks with higher amplitude in the envelope spectrum of the outer ring fault signal, namely, 105.5 Hz, 216.8 Hz, and 322.3 Hz. The above three peaks are very close to the fault frequency, the 2 doubling frequency, and the 3 doubling frequency of the bearing outer ring fault feature. Although the amplitude of the interference spectrum in other places has been effectively weakened, there are still many peaks in the envelope spectrum that are independent of the fault characteristic

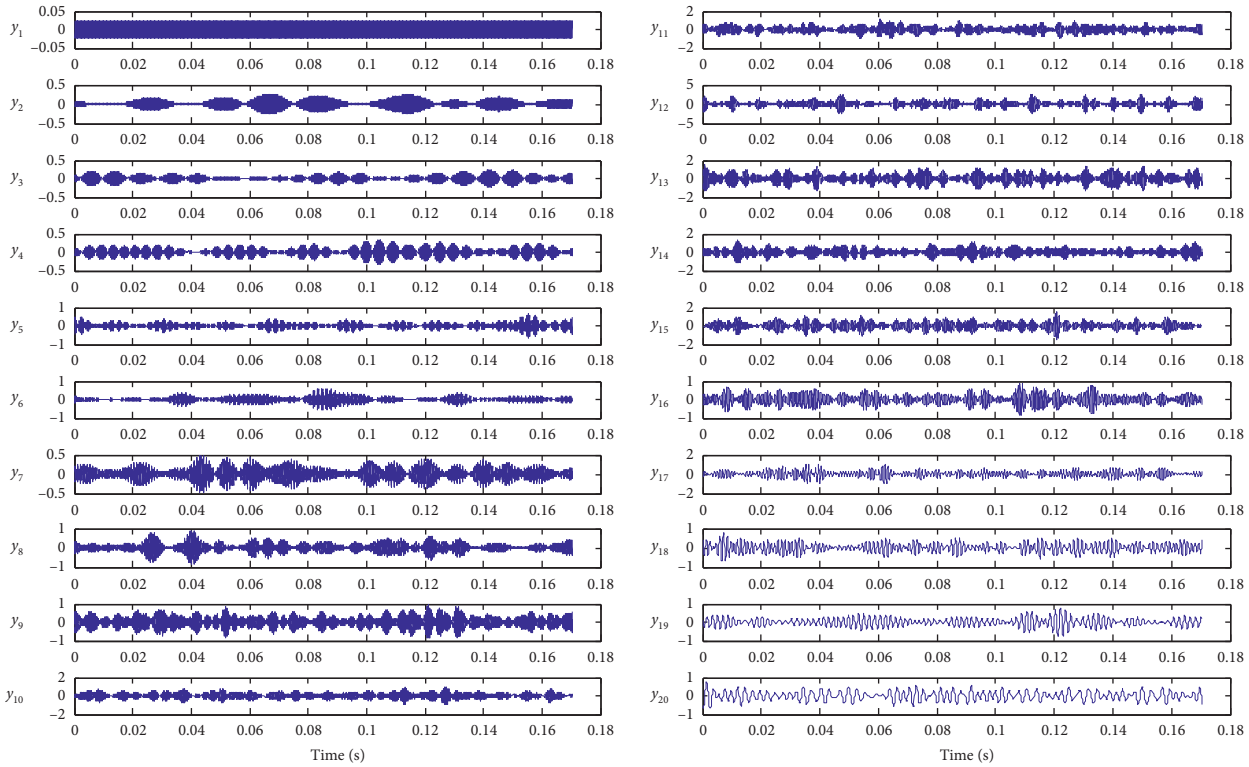

Figure 22: FDM decomposition result.

frequency, which will affect the fault diagnosis results. Therefore, the periodic impact components in the noise reduced signal will be further extracted through the MOMEDA filtering method, and the extraction results are shown in Figure 25.

It can be clearly seen from Figure 26 that the periodic fault impact component of the outer ring fault signal has been extracted. The peak value of the fault characteristic frequency is higher, and the amplitude of the signal component independent of fault impulse is lower. From Figure 26, not only the fault frequency (105.5 Hz) of the bearing outer ring can be clearly distinguished but also the 2 doubling frequency (216.8 Hz), 3 doubling frequency (322.3 Hz), 4 doubling frequency (427.7 Hz), 5 doubling frequency (539.1 Hz), 6 doubling frequency (644.5 Hz), and so on, can be clearly seen, which are very close to the fault characteristic frequency and the doubling frequency calculated theoretically. Therefore, the fault of the bearing outer ring can be accurately diagnosed.

5.3. Rolling Element Signal Analysis of CWRU Bearings. The time domain and the frequency domain of the bearing rolling element fault signal are shown in Figure 26, and the periodic pulse characteristics can be seen from the figure. After adding Gaussian white noise with a signal-to-noise ratio of −5 dB to the rolling element fault signal, the time domain and the frequency domain of the generated mixed signal are shown in Figure 27. Due to the interference of noise, it is difficult to extract the fault feature frequency from the time domain and the frequency domain.

Then, the FDM method is used to decompose the mixed signal of the rolling element with added noise, and 25 FIBF components are obtained. The decomposition results are shown in Figure 28. Due to the limitation of the length of the article, only the first 20 FIBF components are listed in Figure 28. By calculating the cross-correlation coefficient and kurtosis value of each signal component, the results are shown in Table 9. By comparing the data in Table 9, it can be seen that only the y_9 signal component meets the set threshold conditions. Therefore, y_9 component is extracted to reconstruct the target signal channel, and the remaining components are reconstructed as the virtual noise channel. Through the RobustICA for blind source separation, the time-domain waveforms of two groups of independent components are obtained, and the results are shown in Figure 29.

After comparing Figures 29 and 27, it can be seen that the impact component in the signal has been shown through blind source separation. In order to further compare the effect of noise reduction, Hilbert envelope spectrum analysis is carried out for the separated target signal and the mixed signal with −5 dB noise added. The results are shown in Figure 30. Through the analysis of Figure 30, it can be seen that due to the interference of noise, the amplitude of lines in the envelope spectrum of the rolling element fault signal is low, so it is difficult to extract the fault characteristic frequency. After the noise reduction by RobustICA, there are many peaks with high amplitude in the envelope spectrum. The following frequencies can be extracted from the envelope spectrum: 140.6 Hz, 281.3 Hz, and 562.5 Hz. The above frequencies are very close to the theoretical calculated values

Table 8: The correlation coefficient and kurtosis between the FIBF and the original signal.

	y_1	y_2	y_3	y_4	y_5	y_6	y_7	y_8	y_9	y_{10}	y_{11}	y_{12}	y_{13}	y_{14}	y_{15}	y_{16}	y_{17}	y_{18}	y_{19}	Y_{20}	y_{21}	y_{22}	y_{23}	y_{24}	y_{25}
$C(t)$	0.018	0.091	0.074	0.097	0.132	0.116	0.125	0.165	0.217	0.217	0.260	0.523	0.349	0.269	0.277	0.186	0.214	0.163	0.159	0.182	0.086	0.139	0.064	0.034	0.000
$K(t)$	1.000	2.203	2.209	2.266	3.145	4.288	2.564	4.142	2.750	2.872	2.683	4.184	2.981	2.995	3.277	3.013	3.385	2.652	3.151	2.489	2.652	4.111	2.615	2.652	1.000

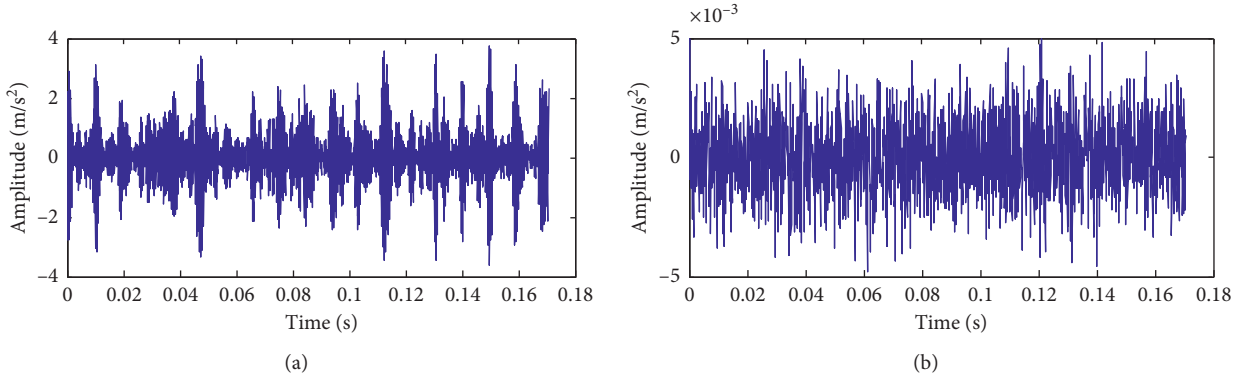

Figure 23: The waveform of each independent component. (a) The waveform of the target signal. (b) The waveform of the noise signal.

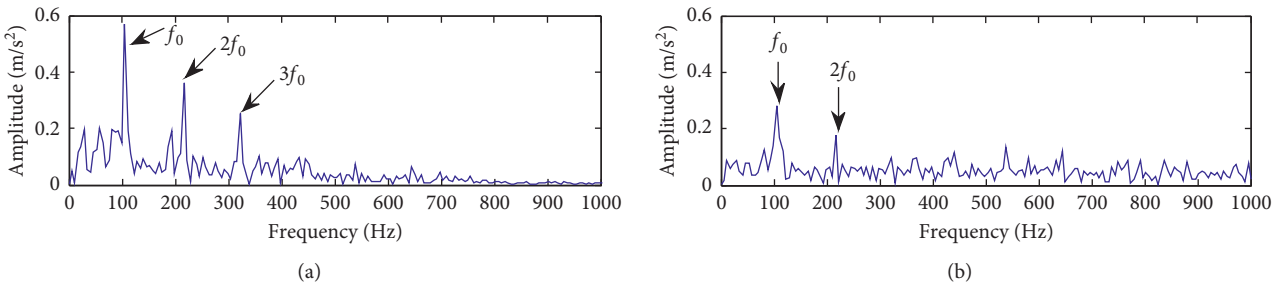

Figure 24: Envelope spectrum analysis. (a) Envelope spectrum analysis of the target signal denoised by FDM-RobustICA. (b) Envelope spectrum of the mixed signal.

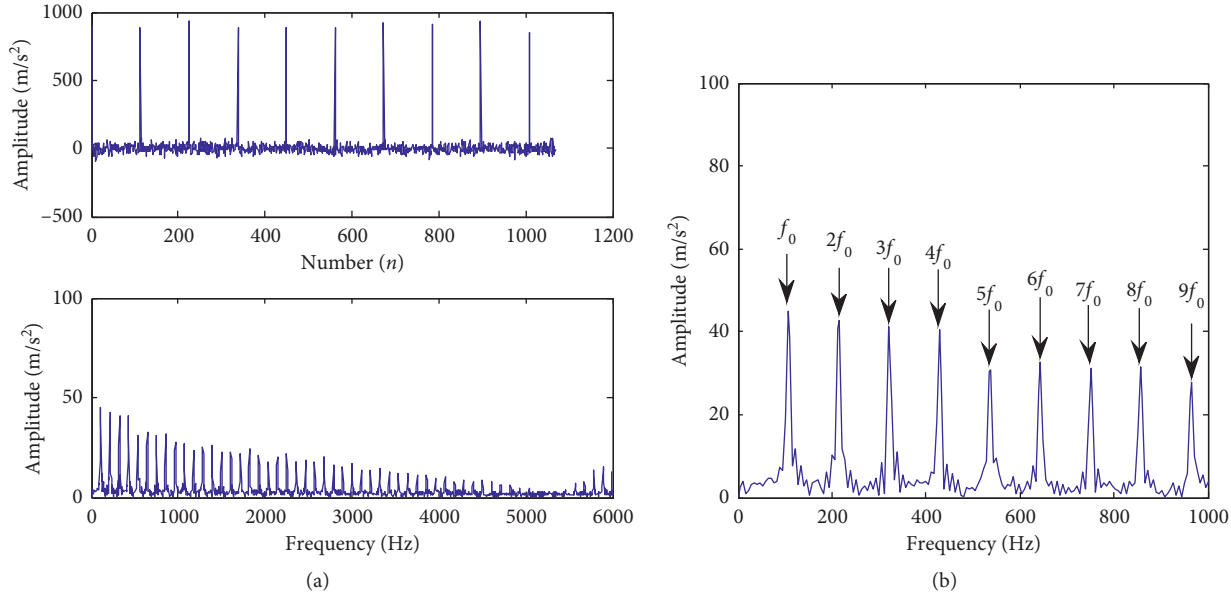

Figure 25: The outer ring MOMEDA filter signal and its envelope spectrum. (a) Time-domain waveform and the envelope spectrum of the MOMEDA filter signal. (b) Part band envelope spectrum of the MOMEDA filter signal.

of the rolling element fault characteristic frequency of 141.1693 Hz, 2 doubling frequency, and 4 doubling frequency. Although the fault characteristic frequency in the envelope spectrum has appeared, there are still many unrelated peaks of the fault characteristic frequency, and the amplitude is large. This brings a certain degree of interference to the fault diagnosis. Therefore, the periodic impact components in the signal after noise reduction will be

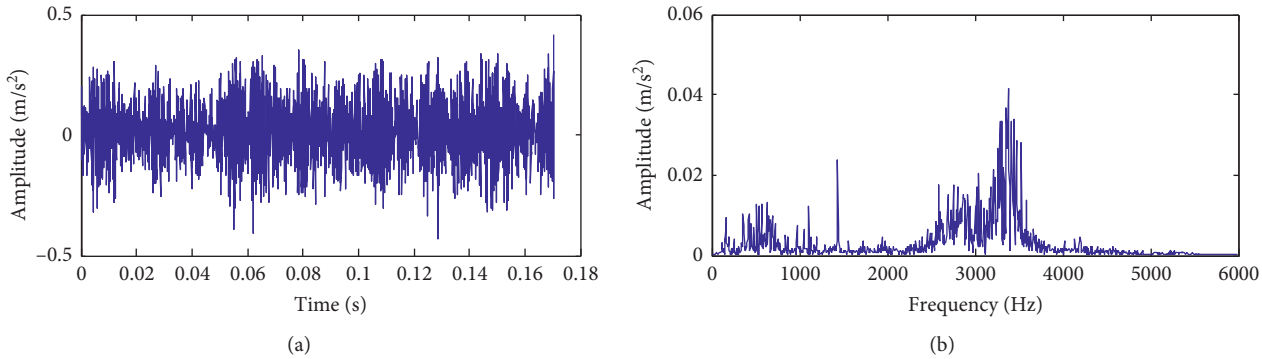

Figure 26: (a) Time-domain analysis and (b) frequency-domain analysis of the original rolling element fault signal.

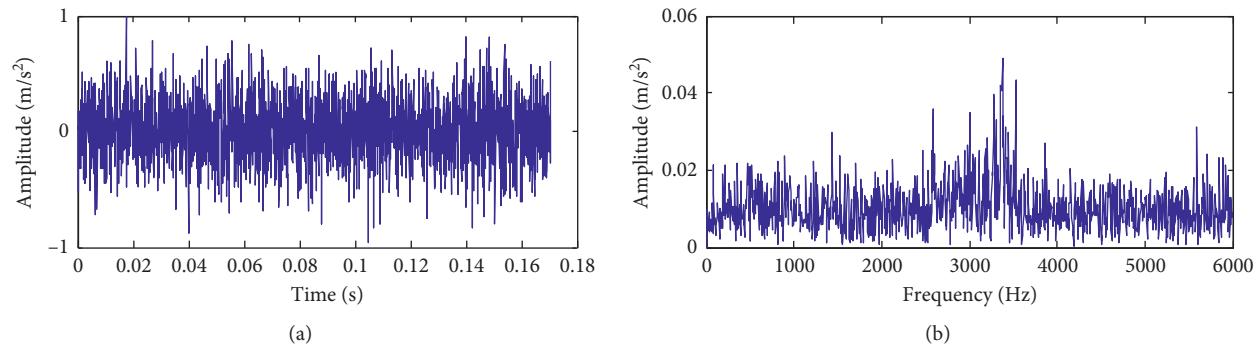

Figure 27: (a) Time-domain analysis and (b) frequency-domain analysis of the mixed signal with SNR = −5 dB.

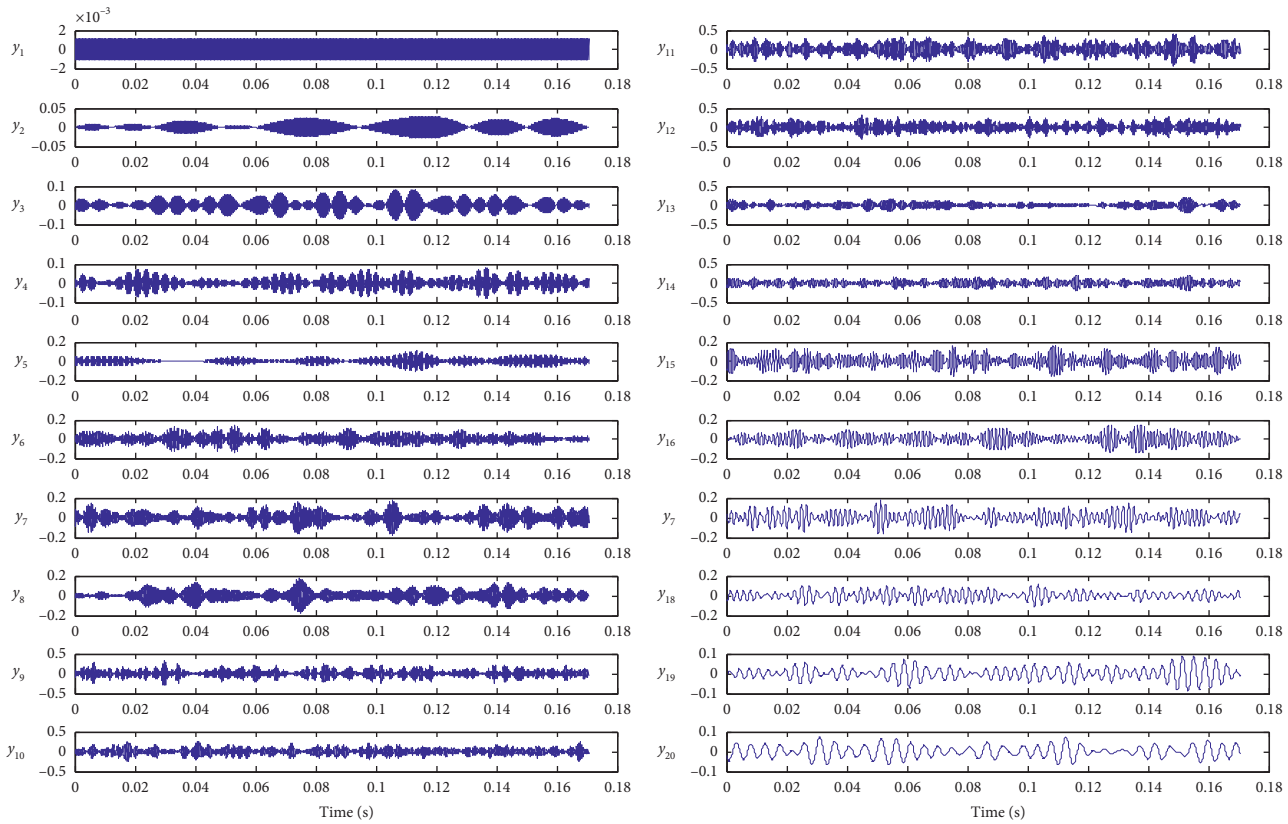

Figure 28: FDM decomposition result.

Table 9: The correlation coefficient and kurtosis between the FIBF and the original signal.

	y_1	y_2	y_3	y_4	y_5	y_6	y_7	y_8	y_9	y_{10}	y_{11}	y_{12}	y_{13}	y_{14}	y_{15}	y_{16}	y_{17}	y_{18}	y_{19}	y_{20}	y_{21}	y_{22}	y_{23}	y_{24}	y_{25}
$C(t)$	0.004	0.054	0.126	0.116	0.120	0.171	0.196	0.173	0.306	0.296	0.490	0.379	0.219	0.254	0.206	0.181	0.209	0.154	0.113	0.107	0.051	0.088	0.017	0.025	0.000
$K(t)$	1.000	2.071	2.276	2.456	3.148	2.712	3.194	3.435	3.276	2.962	2.716	2.684	3.304	2.640	2.710	2.783	2.614	2.591	3.079	2.435	2.673	2.646	2.107	1.500	1.000

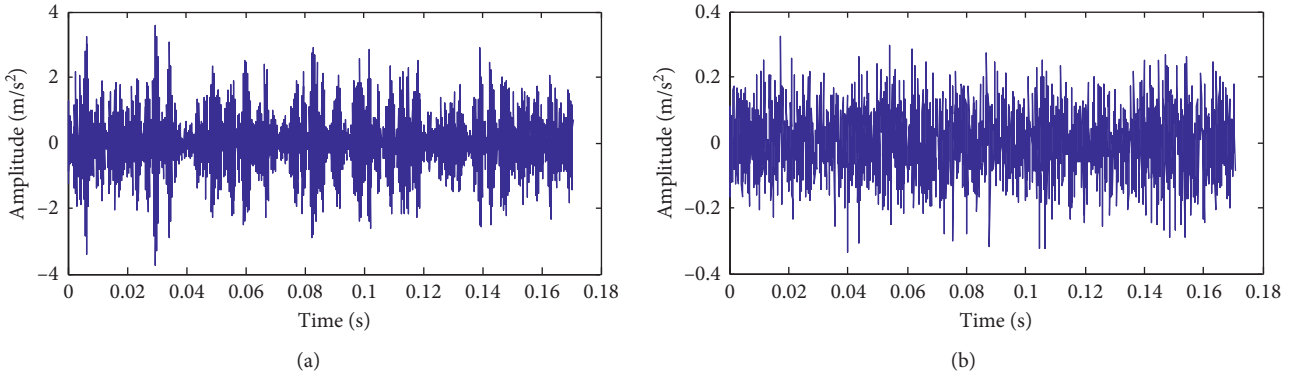

Figure 29: The waveform of each independent component. (a) The waveform of the target signal. (b) The waveform of the noise signal.

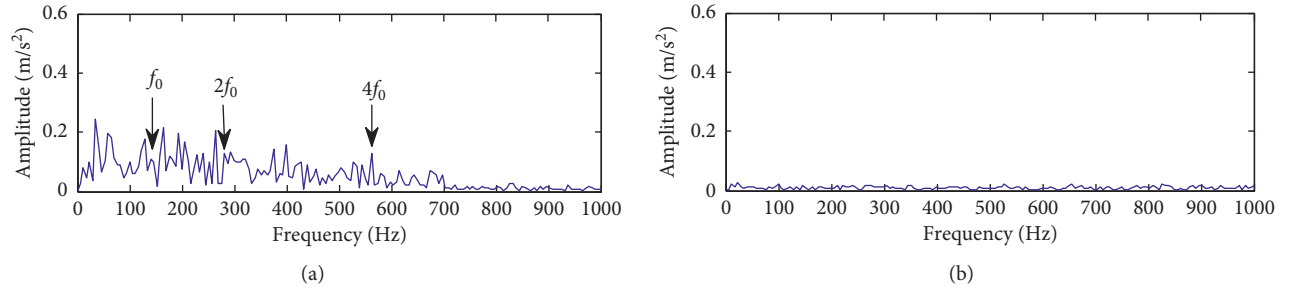

Figure 30: Envelope spectrum analysis. (a) Envelope spectrum analysis of the target signal denoised by FDM-RobustICA. (b) Envelope spectrum of the mixed signal.

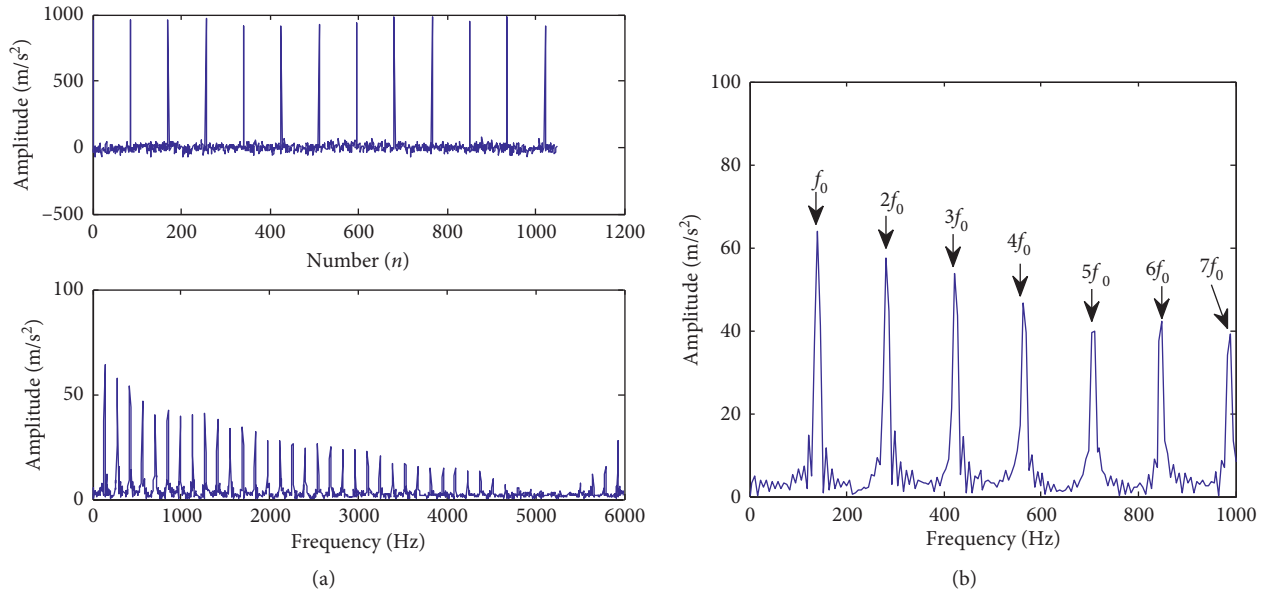

Figure 31: The rolling element MOMEDA filter signal and its envelope spectrum. (a) Time-domain waveform and the envelope spectrum of the MOMEDA filter signal. (b) Part band envelope spectrum of the MOMEDA filter signal.

further extracted by MOMEDA filtering, and the extraction results are shown in Figure 31.

It can be clearly seen from Figure 31 that the periodic fault shock component of the rolling element fault signal is successfully extracted. The peak value of the characteristic frequency of the fault is greatly improved, and the amplitude of the signal component unrelated to the impact of the fault is lower. From Figure 31, not only the frequency of the bearing rolling element fault (140.6 Hz) can be clearly distinguished but also the doubling frequency such as the 2

doubling frequency (281.3 Hz), 3 doubling frequency (421.9 Hz), 4 doubling frequency (562.5 Hz), 5 doubling frequency (703.1 Hz), and 6 doubling frequency (843.6 Hz) are clearly visible, which are very close to the fault characteristic frequency and the multiple frequency theoretically. Therefore, the fault of the bearing rolling element can be accurately diagnosed.

6. Conclusions

Aiming at the problem of fault feature extraction of vibration signals of rolling bearings under the background of strong noise, this paper proposes a fault feature extraction method based on the combination of FDM-RobustICA and MOMEDA. After the experimental analysis of the constructed simulation signals and the actual bearing fault signals, the conclusions reached are as follows:

(1) On the basis of cross-correlation analysis and kurtosis, the signal components obtained by the FDM method are selected to reconstruct the observation signal channel and the virtual noise channel, which not only avoid the mode overlapping and endpoint effect produced by traditional methods but also solve the problem that RobustICA cannot process the single-channel signal and the lack of fault information caused by blind selection of signal components.

(2) By comparing the results of the proposed method with the traditional method of LMD-RobustICA and ITD-RobustICA, the results show that the proposed method can more effectively separate fault signals and noise signals and has achieved relative better evaluation index value.

(3) By using MOMEDA to filter the noise reduced signal, the periodic impact component under the strong noise background can be effectively enhanced, and the irrelevant impact signal can be weakened. Based on the constructed simulation signals and the experimental analysis of the inner ring, outer ring, and rolling element of rolling bearings, the results show that the proposed method can accurately extract the characteristic frequency of faults in a strong noise background environment, and the amplitude is more obvious. In our future work, we will consider more reasonable approaches to optimize the parameters of the proposed method and add other denoising techniques.

Data Availability

The data used to support the findings of this study are available from the corresponding author upon request.

Conflicts of Interest

The authors declare that there are no conflicts of interest regarding the publication of this paper.

Acknowledgments

This work was supported by the Joint Special Fund for Basic Research of Local Universities in Yunnan Province (no. 2019FH001-121) and Science Research Fund Project of Baoshan University (no. BYBS201802).

References

[1] P. Schniter, "Short-time fourier transform," *Advanced Topics in Signal Processing*, vol. 32, pp. 289–337, 2009.

[2] D. Griffin and J. S. Jae Lim, "Signal estimation from modified short-time fourier transform," *IEEE Transactions on Acoustics, Speech, and Signal Processing*, vol. 32, no. 2, pp. 236–243, 1984.

[3] A. Georgakis, L. K. Stergioulas, and G. Giakas, "Wigner filtering with smooth roll-off boundary for differentiation of noisy non-stationary signals," *Signal Processing*, vol. 82, no. 10, pp. 1411–1415, 2002.

[4] M. Holschneider, R. Kronland-Martinet, J. Morlet, and P. Tchamitchian, *A Real-Time Algorithm for Signal Analysis with the Help of the Wavelet Transform*, Springer, Berlin, Germany, 1989.

[5] Z. Nenadic and J. W. Burdick, "Spike detection using the continuous wavelet transform," *IEEE Transactions on Biomedical Engineering*, vol. 52, no. 1, pp. 74–87, 2005.

[6] N. E. Huang, Z. Shen, S. R. Long et al., "The empirical mode decomposition and the Hilbert spectrum for nonlinear and non-stationary time series analysis," *Proceedings of the Royal Society of London. Series A: Mathematical, Physical and Engineering Sciences*, vol. 454, no. 1971, pp. 903–995, 1998.

[7] V. K. Wu, V. Bajaj, A. Kumar, D. Sharma, and G. K. Singh, "An efficient method for analysis of EMG signals using improved empirical mode decomposition," *AEU-International Journal of Electronics and Communications*, vol. 72, pp. 200–209, 2017.

[8] J. Cheng, D. Yu, J. Tang, and Y. Yang, "Application of frequency family separation method based upon EMD and local Hilbert energy spectrum method to gear fault diagnosis," *Mechanism and Machine Theory*, vol. 43, no. 6, pp. 712–723, 2008.

[9] Z. Wu and N. E. Huang, "Ensemble empirical mode decomposition: a noise-assisted data analysis method," *Advances in Adaptive Data Analysis*, vol. 1, no. 1, pp. 1–41, 2009.

[10] H. Li, T. Liu, X. Wu, and Q. Chen, "Application of EEMD and improved frequency band entropy in bearing fault feature extraction," *ISA Transactions*, vol. 88, pp. 170–185, 2019.

[11] C. Wu, J. Wu, and J. Yang, "Research on fault diagnosis of check valve based on CEEMD compound screening and improved SECPSO," *Journal of Computers*, vol. 30, pp. 128–144, 2019.

[12] K. Moshen, C. Gang, P. Yusong, and Y. Li, "Research of planetary gear fault diagnosis based on permutation entropy of CEEMDAN and ANFIS," *Sensors*, vol. 18, no. 3, p. 782, 2018.

[13] J. S. Smith and S. Jonathan, "The local mean decomposition and its application to EEG perception data," *Journal of the Royal Society Interface*, vol. 2, no. 5, pp. 443–454, 2005.

[14] M. G. Frei and I. Osorio, "Intrinsic time-scale decomposition: time-frequency-energy analysis and real-time filtering of non-stationary signals," *Proceedings of the Royal Society A: Mathematical, Physical and Engineering Sciences*, vol. 463, no. 2078, pp. 321–342, 2007.

[15] P. Singh, S. D. Joshi, R. K. Patney, and K. Saha, "The fourier decomposition method for nonlinear and non-stationary time series analysis," *Proceedings of the Royal Society A: Mathematical, Physical and Engineering Science*, vol. 473, pp. 1–12, 2017.

[16] C. H. Dou and J. S. Lin, "Extraction of fault features of machinery based on fourier decomposition method," *IEEE Access*, vol. 7, pp. 1–11, 2019.

[17] Y. Liu, X. D. Liu, and S. Liang, "Aeroengine rotor fault diagnosis based on fourier decomposition method," *China Mechanical Engineering*, vol. 30, pp. 2156–2163, 2019.

[18] X. W. Fu and X. Q. Gao, "Rolling bearing fault diagnosis based on FDM and singular value difference spectrum," *Acta Metrologica Sinica*, vol. 39, pp. 688–692, 2018.

[19] P. Comon, "Independent component analysis, a new concept?" *Signal Processing*, vol. 36, no. 3, pp. 287–314, 1994.

[20] A. Hyvärinen and E. Oja, "A fast fixed-point algorithm for independent component analysis," *Neural Computation*, vol. 9, no. 7, pp. 1483–1492, 1997.

[21] A. Hyvärinen, "Fast and robust fixed-point algorithms for independent component analysis," *IEEE Transactions on Neural Networks*, vol. 10, no. 3, pp. 626–634, 1999.

[22] P. Chevalier, L. Albera, P. Comon, and A. Ferreol, "Comparative performance analysis of eight blind source separation methods on radio communications signals," in *Proceedings of the International Joint Conference on Neural Networks*, pp. 25–31, Budapest, Hungary, July 2004.

[23] V. Zarzoso and P. Comon, "Robust independent component analysis for blind source separation and extraction with application in electrocardiography," in *Proceedings of the EMBC-2008, 30th Annual International Conference of the IEEE Engineering in Medicine and Biology Society*, pp. 3344–3347, Vancouver, BC, Canada, August 2008.

[24] V. Zarzoso and P. Comon, "Robust independent component analysis by iterative maximization of the kurtosis contrast with algebraic optimal step size," *IEEE Transactions on Neural Networks*, vol. 21, pp. 248–261, 2009.

[25] J. Yao, Y. Xiang, S. Qian, S. Wang, and S. Wu, "Noise source identification of diesel engine based on variational mode decomposition and robust independent component analysis," *Applied Acoustics*, vol. 116, pp. 184–194, 2017.

[26] F. Bi, L. Li, J. Zhang, and T. Ma, "Source identification of gasoline engine noise based on continuous wavelet transform and EEMD-RobustICA," *Applied Acoustics*, vol. 100, pp. 34–42, 2015.

[27] Y. Jiachi, X. Yang, Q. Sichong, and W. Shuai, "Radiation noise separation of internal combustion engine based on Gammatone-RobustICA method," *Shock and Vibration*, vol. 2017, Article ID 7565041, 14 pages, 2017.

[28] Y. Jingzong, W. Xiaodong, W. Jiande, and F. Zao, "A noise reduction method based on CEEMD-RobustICA and its application in pipeline blockage signal," *Journal of Applied Science and Engineering*, vol. 22, pp. 1–10, 2019.

[29] Y. Jiachi, X. Yang, Q. Sichong, and W. Shuai, "Noise source separation of an internal combustion engine based on a single-channel algorithm," *Shock and Vibration*, vol. 2019, Article ID 1283263, 19 pages, 2019.

[30] H. Weixin and L. Dunwen, "Mine microseismic signal denosing based on variational mode decomposition and independent component analysis," *Journal of Vibration and Shock*, vol. 38, pp. 56–63, 2019.

[31] R. A. Wiggins, "Minimum entropy deconvolution," *Geoexploration*, vol. 16, no. 1-2, pp. 21–35, 1978.

[32] S. Wang and J. Xiang, "A minimum entropy deconvolution-enhanced convolutional neural networks for fault diagnosis of axial piston pumps," *Soft Computing*, vol. 24, no. 4, pp. 2983–2997, 2020.

[33] H. Liu and J. Xiang, "A strategy using variational mode decomposition, L-kurtosis and minimum entropy deconvolution to detect mechanical faults," *IEEE Access*, vol. 7, pp. 70564–70573, 2019.

[34] N. Sawalhi, R. B. Randall, and H. Endo, "The enhancement of fault detection and diagnosis in rolling element bearings using minimum entropy deconvolution combined with spectral kurtosis," *Mechanical Systems and Signal Processing*, vol. 21, no. 6, pp. 2616–2633, 2007.

[35] G. L. McDonald, Q. Zhao, and M. J. Zuo, "Maximum correlated kurtosis deconvolution and application on gear tooth chip fault detection," *Mechanical Systems and Signal Processing*, vol. 33, pp. 237–255, 2012.

[36] G. L. Mcdonald and Q. Zhao, "Multipoint optimal minimum entropy deconvolution and convolution fix: application to vibration fault detection," *Mechanical Systems and Signal Processing*, vol. 82, pp. 461–477, 2017.

[37] Y. Li, G. Cheng, X. Chen, and Y. Pang, "Research on bearing fault diagnosis method based on filter features of MOML-MEDA and LSTM," *Entropy*, vol. 21, pp. 1–15, 2019.

[38] W. A. Smith and R. B. Randall, "Rolling element bearing diagnostics using the Case Western Reserve University data: a benchmark study," *Mechanical Systems and Signal Processing*, vol. 64-65, pp. 100–131, 2015.

[39] J. Xia, L. Zhao, Y. Bai, M. Yu, and Z. Wang, "Feature extraction for rolling element bearing weak fault based on MCKD and VMD," *Journal of Vibration and Shock*, vol. 36, pp. 78–83, 2017.